Master of Science Thesis
VT2024

Estimation of Uncertainties in Radioiodine Uptake Measurement and Thyroid Volume Scintigraphy Before Subsequent Radioiodine Therapy

Louise Alminde

Supervisors

Jimmy Börjesson and Anna Sörensson

Medical Radiation Physics, Lund
Medical Physics Programme
Faculty of Science
Lund University, Sweden
www.msf.lu.se

Populärvetenskaplig sammanfattning

Hypertyreos är en sköldkörtelsjukdom där sköldkörteln är överaktiv och producerar för mycket hormoner. Tillståndet kan orsaka symptom som är jobbiga att leva med i vardagen, till exempel hjärtklappning, svettningar, yrsel och illamående. En utav de behandlingar som används mot hypertyreos är radiojodbehandling. Vid radiojodbehandling utnyttjar man sköldkörtelns egenskap att absorbera jod från den kost man äter. Radioaktivt jod, närmare bestämt isotopen ^{131}I, ger en lokal stråldos till sköldkörteln. Det är den ansvarige läkarens roll att ordinera vilken stråldos (måldos) sköldkörteln ska få och det är av yttersta vikt att den bestäms så noggrant som möjligt, för att patienten inte skall erhålla en för hög eller låg måldos.

Utifrån läkarens ordination av måldos beräknas den administrerade aktiviteten, baserad på hur mycket jod sköldkörteln tar upp och på hur stor volym av sköldkörteln som aktivt tar upp jod. Vilken andel jod sköldkörteln tar upp jämfört mot vad som har intagits i kroppen beräknas med hjälp av så kallade upptagsmätningar. Den aktiva volymen av sköldkörteln bestäms utifrån nuklearmedicinska bilder. Ett lågt upptag av jod och en stor sköldkörtel innebär att det krävs en högre behandlade dos.

Detta arbete har studerat osäkerheterna vid uppskattningar av jodupptaget och sköldkörtelvolymen på grund av dess påverkan på måldosen. Experimentella mätningar har utförts på system och utrustning som används kliniskt för upptagsmätning och volymsuppskattning vid Hallands sjukhus, Halmstad. Inverkan av hur detektorn är positionerad vid upptagsmätningen samt betydelsen av sköldkörtelns storlek och fördelning av radioaktivt jod inom densamma har studerats. 3D-utskrivna sköldkörtelfantom användes för att utvärdera befintlig metod för att uppskatta sköldkörtelvolymerna. Dessutom undersöktes möjligheten att byta ut den subjektiva volymsbestämningen mot en mer automatiserad och objektiv metod.

Resultaten visade att uppskattningen av jodupptaget påverkas av en felplacering av detektorn relativt sköldkörteln, men att felplaceringen måste vara större än 5 cm för att ha en större påverkan än 10% på det uppskattade värdet. Detta skulle innebära en ökning på 11% av måldosen. Vidare visade det sig att uppskattningen av jodupptaget kan minska med upp till 35% om all radioaktiv substans är på ett kliniskt relevant djup av 30 mm, vilket motsvarar 54% för hög måldos. Den befintliga mätuppställningen visade sig ha störst påverkan på uppskattningen av jodupptaget, med upp till 27% ökning. Detta resulterar i en 21% för låg måldos. De uppskattade fantomvolymerna visade sig variera stort beroende på vilka bildinställningar som gjordes vid den subjektiva uppskattningen. Den maximala avvikelsen av uppskattad fantomvolym var -36%, vilket motsvarar 36% för låg måldos, men de flesta hade betydligt mindre avvikelse än så.

En slutsats av studien är att uppskattningen av jodupptaget beror på flera av de faktorer som studerats. Metoden för upptagsmätningar kan behöva modifieras för att öka noggrannheten. En annan slutsats var att den subjektiva metoden för uppskattning av sköldkörtelvolymen ger stora skillnader mellan olika personer. Ett alternativ kan då vara att införa en objektiv automatisk volymsuppskattning, via en optimeringsinsats, vilken dock låg utanför målet med denna studie.

Abstract

Aim: The aim was to estimate the uncertainty of various factors, influencing the radioiodine uptake (RAIU) at clinical measurements of hyperthyroid patients. Furthermore, to evaluate the estimation of thyroid volume from nuclear medicine scintigraphic images. Another aim was to investigate in what extent these uncertainties may influence the eventual therapeutic radioiodine activity, and thereby the absorbed target dose to the thyroid gland.

Background: Hyperthyroidism is a condition where the thyroid gland produces excess amounts of thyroid hormones and the affected patient may experience substantial symptoms. Clinically, various treatment procedures are available, with high-dose radioiodine being a straightforward alternative. The activity, sufficient to reach the clinically prescribed absorbed dose level in the thyroid gland, is largely influenced by the estimated radioiodine uptake in the gland but also by the estimated gland volume. A number of subfactors are involved in the process of producing the uptake and gland volume estimates. Some of these were accounted for in the present study. The project follows the locally used technique at the Halland Hospital Halmstad, Sweden: radioiodine uptake, using a trace amount of the ^{131}I isotope, together with planar scintigraphy using Technetium pertechnetate as tracer.

Materials and Method: Fillable and reusable 3D-printed thyroid phantoms were used to reflect the uptake of iodine and technetium in the thyroid gland. The uncertainty in uptake measurement, due to the source position, the source depth and the presence of an air gap in the setup was investigated. The uncertainty in the estimated gland volume is largely influenced by the technique used to discriminate between background and gland tissue. The presently used technique with medical physicists evaluating planar, scintigraphic, images, using subjectively, hand-drawn regions of interest (ROI), was compared, for various phantom models, with an automatic segmentation technique and a fixed discrimination level. An analogous approach was used for the simulated SPECT images.

Results: The RAIU value was seen to deviate, by up to 10%, if the detector was mispositioned by up to 5 cm. This resulted in a, theoretically, 11% higher target dose. The RAIU value was also noted to deviate by up to 35%, depending on the depth to the position of the activity, with a maximum deviation for 30 mm. This implied a theoretically 54% higher target dose. Moreover, an air gap present in the system setup, meant that the RAIU value may deviate by up to 27%. This resulted in a theoretically 21% lower target dose. The estimated phantom volumes, based on freehand drawn ROIs, showed a large variation with a maximum deviation of 35%. This in turn implied a theoretically 35% lower target dose. Also noted was that the precision of the estimated phantom volume was higher than the corresponding accuracy. Automatic segmentation of planar scintigraphic images was sensitive to differences in count ratio of thyroid to background. On the other hand, SPECT images were seen to be sensitive to differences in the threshold value.

Conclusions: In this study, various factors clearly influenced both the RAIU and the gland volume estimates. Since the calculated therapeutic iodine activity prescribed for treatment of the patient strongly depends on these two parameters, it is essential that they are determined in an accurate and reproducible manner. The level of influence is not negligible and may, in fact, affect the clinical outcome for the patient. Further studies are needed to add to the complete picture of uncertainty in uptake measurements and nuclear scintigrams. However, as noted, some of the observations in this study also hinted towards possible improvements as to decrease the overall uncertainties.

Acknowledgements

First of all, I would like to express my gratitude to my supervisors Jimmy Börjesson and Anna Sörensson for your encouragement and valuable discussions throughout the course of my Master's thesis.

I would also like to thank:

- Elin Gylling (Medical Physicists at HSH) for bouncing ideas and all your expertise in nuclear medicine.
- The biomedical scientists Ida Lundh, Marcus Nilsson, Evelina Vesik and Stina Lu at the Nuclear Medicine section at HSH for your help with the gamma camera and for your patience during the semester.
- 3D-centrum in Lund, especially Muris Imsirovic, for your help and creative ideas with the thyroid phantoms.
- MTA at HSH, especially Joachim Barkman, for your technical expertise and support with my phantom setups.

Finally, I would like to thank my family and friends from the bottom of my heart for your positive support during my five years of studies.

List of Abbrevations and Acronyms

CR	Average pulse count ratio between thyroid gland (or thyroid phantom) and background
CPS	Counts per second
FOV	Field of view
GD	Graves' disease
HSH	Hallands Sjukhus Halmstad (Halland Hospital Halmstad)
MP	Medical physicsist
PS	Planar scintigraphy
QA	Quality assurance
Radioiodine	Radioactive iodine, ^{131}I
RAIU	Radioiodine uptake
ROI	Region of interest
SPECT	Single photon emission computed tomography
TMNG	Toxic multinodular goiter
TNG	Toxic nodular goiter

Contents

1 Introduction **1**
1.1 Aims . . . 2

2 Background **2**
2.1 The Thyroid Gland . . . 2
2.2 Hyperthyroidism . . . 2
2.3 Theragnostic Procedure of Hyperthyroidism . . . 3
2.3.1 Radioiodine Uptake Measurement . . . 3
2.3.1.1 Quality Assurance of Uptake Measurement System . . . 6
2.3.2 Estimation of Thyroid Gland Volume . . . 6
2.3.2.1 Planar Scintigraphy . . . 6
2.3.2.2 Volume Estimation from Planar Scintigraphic Image . . . 7
2.3.3 Radioiodine Therapy . . . 8
2.3.3.1 Calculation of Activity to Reach the Target Dose . . . 8
2.3.4 Absorbed and Effective Doses from the Theragnostic Procedure . . . 9
2.4 Factors Affecting the Therapeutic Absorbed Dose to the Thyroid Gland . . . 10
2.4.1 Radioiodine Uptake Measurement . . . 10
2.4.2 Thyroid Gland Volume Estimation . . . 12
2.4.3 Other Influencing Factors . . . 13

3 Materials and Method **14**
3.1 Production of Phantoms . . . 14
3.1.1 Phantom Structure . . . 14
3.1.2 Phantom Printing . . . 14
3.1.3 Thyroid Phantom Volumes . . . 15
3.2 Radioiodine Uptake Measurements . . . 16
3.2.1 Source Position Dependence . . . 16
3.2.2 Source Depth Dependence . . . 17
3.2.3 Detector Angle Dependence . . . 17
3.2.4 Air Gap Dependence . . . 18
3.3 Thyroid Phantom Estimation using Scintigraphic Methods . . . 18
3.3.1 Phantom Preparations . . . 18
3.3.2 Scintigraphic Scan with Gamma Camera . . . 20
3.3.3 Pulse Count Ratios in Scintigraphic Images . . . 20
3.3.4 Thyroid Phantom Volume Estimation from Scintigraphic Scans . . . 21
3.3.4.1 Estimated Thyroid Phantom Volumes from Freehand Drawn ROIs . 22
3.3.4.2 Estimated Thyroid Phantom Volumes from Automatic Segmentation 22

4 Results **24**
4.1 Uptake Measurements . . . 24
4.1.1 Source Position Dependence . . . 24
4.1.2 Source Depth Dependence . . . 25
4.1.3 Detector Angle Dependence . . . 26
4.1.4 Air Gap Dependence . . . 27

4.2 Thyroid Phantom Volume Estimation . . . 28
4.2.1 Count ratio (CR) of gland to background ROIs . . . 28
4.2.2 Estimated Thyroid Phantom Volumes from Freehand Drawn ROIs . . . 29
4.2.2.1 Phantom Models A . . . 29
4.2.2.2 Phantom Model B . . . 31
4.2.3 Estimated Thyroid Phantom Volumes from Automatically Segmented PS Images . . . 32
4.2.3.1 Phantom Models A . . . 32
4.2.3.2 Phantom Model B . . . 34
4.2.4 Estimated Thyroid Phantom Volumes from Automatically Segmented SPECT Images . . . 34
4.2.4.1 Phantom Models A . . . 34
4.2.4.2 Phantom Model B . . . 36
4.2.5 Summary of Estimated Phantom Volumes . . . 36

5 Discussion **38**
5.1 Uptake Measurements . . . 38
5.1.1 Source Position Dependence . . . 38
5.1.2 Source Depth Dependence . . . 38
5.1.3 Detector Angle Dependence . . . 38
5.1.4 Air Gap Dependence . . . 39
5.2 Volume Estimation . . . 39
5.2.1 CR Values . . . 39
5.2.2 Window Settings . . . 39
5.2.3 Estimated Volumes from Freehand Drawn ROIs . . . 40
5.2.4 Estimated Volumes from Automatic Segmentation . . . 41

6 Conclusions **43**
6.1 RAIU Value . . . 43
6.2 Estimated Phantom Volumes . . . 43

7 Future Work **43**

A Gamma Camera Settings and Acquisitions Parameters **47**

B Matrix for Uptake Measurements **48**

C Planar Scintigraphic Images **49**

1 Introduction

Every year, around 3,500 people in Sweden are diagnosed with hyperthyroidism. Hyperthyroidism is a condition in which the thyroid gland produces an excess of thyroid hormones caused by a benign thyroid disorder. The excess of thyroid hormones may cause anxiety, weight loss, palpitations, increased heart rate, fatigue and sweating, among other symptoms [1].

The treatment alternatives for hyperthyroidism are commonly antithyroid medicine, surgery and radioactive iodine therapy (radioiodine therapy), all with the purpose to reduce the thyroid hormone levels. Radioiodine therapy is the most cost-effective alternative and is also relatively straight forward. Radiotherapy requires less resources compared with surgery. Also, radioactive medication is less expensive than antithyroid drugs which may have to be taken for the rest of life. In addition, radioiodine therapy is a safe (e.g. avoiding surgical complications) and effective method, and is in some cases considered the first line treatment if no contraindications are found [2, 3, 4].

^{131}I is the radioactive isotope used for modern radiotherapy of hyperthyroidism. It is suitable for therapy of hyperthyroidism because of its biological and physical properties. Iodine is naturally absorbed and retained by the thyroid gland. The half-life of ^{131}I is 8.02 days and it decays by β-particle emission, where the most common average β-particle energy is 0.192 MeV [5]. Furthermore, the average range of the β-particle is 0.4 mm and thus the energy is deposited near the decay location [4]. Also, a useful γ-ray is emitted with the energy of 365 keV [5], which can be used for diagnostic purposes. To summarize, ^{131}I is a suitable theragnostic radio nuclide for treatment of hyperthyroidism [4].

According to the ALARA principle (As low as reasonably achievable), the goal is to minimize the absorbed dose to all organs and tissues except to the thyroid gland which should receive the target dose required for reduction of the thyroid hormones. Therefore, it is of great interest to optimize the radioiodine therapy as well as characterize and determine the uncertainties of the given treatment.

When the prescribed target dose to the thyroid gland is decided (depending on diagnosis), the amount of radioactive iodine to be administrated depends on

- the effective half-life of iodine in the thyroid gland,
- the radioiodine uptake (RAIU) in the thyroid gland and
- the volume of the thyroid gland absorbing radioiodine.

These parameters all vary between patients [6] and, since the treatment is individually adapted to every patient, the parameters need to be accurately estimated to deliver the desired target dose to the thyroid gland. The effective half-life and the RAIU value are estimated by pre-therapeutic uptake measurements. The active volume of the thyroid gland can be estimated with a scintigraphy scan based on technetium pertechnetate, $^{99m}TcO_4^-$, which have the same distribution in the thyroid gland as iodine [4, 7]. These methods are used both to diagnose hyperthyroidism and for determination of the activity for the subsequent radiotherapy (theragnostic method)[4, 8, 9].

1.1 Aims

The aim of this project was to characterize and determine uncertainties in factors influencing the accuracy of the calculated administrated target dose to the thyroid gland in relation to the prescribed target dose. The project focused on two procedures; i) the RAIU value from thyroid radioiodine (^{131}I) uptake measurements and ii) thyroid gland volume estimation from scintigraphic images with technetium pertechnetate. Moreover, factors influencing the outcome of these procedures were to be identified and, in some cases, studied in more detail. In particular, the local methods at the Nuclear Medicine section, Diagnostic Radiology, at the Halland Hospital Halmstad (HSH) were investigated.

2 Background

2.1 The Thyroid Gland

The thyroid gland belongs to the endocrine system. The gland is located at the front of the neck, straddling the trachea. Generally, it has the shape of a butterfly with two lobes and a middle part, the isthmus, connecting the two lobes [11] (see Figure 2.1). A normally functioning thyroid gland has a vertical diameter of 5-8 cm and each lobe width is about 2-4 cm. The weight is about 20 g, as an average value for the Western European population [12]. It is located 5-10 mm under the skin, muscles and nerves [12].

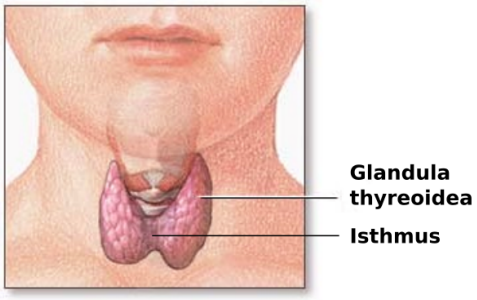

Figure 2.1: The thyroid gland with lobes, situated close to the trachea. The connection isthmus is also indicated [10].

The thyroid gland produces hormones that control, for example metabolism, heart rate and body temperature. The triiodothyronine (T3) hormone has the greatest effect on these body functions, while the thyroxine (T4) hormone, which is produced in the greatest quantity, can be converted into T3 hormone. Reverse triiodothyronine (RT3) has the opposite role compared to T3 hormone. For hormone production, iodine is necessary and is absorbed from food and water. The production of thyroid hormones is controlled by the hypothalamus. It produces thyroid-releasing hormone, which is a signal for the pituitary gland to produce thyroid-stimulating hormone (TSH), which in turn stimulates the thyroid gland to produce T3 and T4. The thyroid gland only produces T3 and T4 when sufficient iodine is available [11].

2.2 Hyperthyroidism

There are several conditions and disorders associated with the thyroid gland function. The ones relevant for this work are different types of hyperthyroidism, which is a collective name for benign disorders in which the gland is overactive, i.e. produces thyroid hormones in excess. The disorders that are generally treatable with radioiodine (^{131}I) are Graves' disease (GD), toxic adenoma (TA) and toxic multinodular goiter (TMNG)[4]. The symptoms may differ depending on the diagnose.

Graves' disease (GD) is an autoimmune disease, in which the immune system is triggered to produce an antibody which stimulates the thyroid gland to produce excess amounts of thyroid hormones (T3, T4). TA and TMNG are conditions when there is growth on and in the thyroid gland in the form of one (TA) or more (TMNG) nodules. There are different types of nodules and if the thyroid gland consists of hyperfunctioning nodule(s), it is a case of hyperthyroidism as TA or TMNG [8, 9].

On the contrary, if the patient suffers from infection in the thyroid gland, thyroiditis shows the same symptoms and elevated hormone levels. However, thyroiditis is not hyperthyroidism and iodine uptake is low. Furthermore, the thyroiditis will not show up on scintigraphic images using technetium as a radiotracer (see Figure 2.5). It is worth noting that thyroiditis has different stages and the symptoms and biological process differ between them [13].

2.3 Theragnostic Procedure of Hyperthyroidism

The procedures and systems described in this section are those used at HSH. However, the techniques and equipment are similar those used by other Swedish nuclear medicine departments.

To diagnose hyperthyroidism, blood samples in which the thyroid hormone levels are analyzed, are essential. The pituitary gland will produce less TSH if there is an excess of thyroid hormones, and thus, a low blood level of TSH indicates an hyperfunctioning thyroid gland. However, the TSH levels can be normal even with TA and TMNG. The blood levels of antibodies may also be used to verify GD. If the blood level of TSH is low, the patient may be referred to a nuclear medicine examination. This will add valuable information for the diagnosis regardless of which type of hyperthyroidism the patient suffers from. As hyperthyroidism is often accompanied with an increased radioiodine uptake (RAIU), an uptake measurement of radioiodine is used for quantification. The uptake measurement is often combined with a thyroid scintigraphy scan, using radioactive ^{99m}Tc to study both the distribution of iodine within the thyroid gland and the shape/volume of the thyroid gland. [8, 9]. The physiscian diagnoses the patient on the basis of the information from the blood tests, the patient's symptoms, the RAIU value and the scintigraphic image. The physiscian decides, together with the patient, whether the patient is suitable for radioiodine therapy. If this is the case, the radioiodine activity administered to the patient is calculated on the basis of the radioiodine uptake value, the volume determined from the scintigraphic image and the prescribed target dose. Thus, it is important that the RAIU value and the scintigraphy volume are both accurate.

2.3.1 Radioiodine Uptake Measurement

The amount of iodine absorbed by the thyroid gland largely depends on which thyroid disease the patient suffers from. If the RAIU value is above 25% after five days, this may indicate hyperthyroidism. In addition, an RAIU value in the normal range is not a contraindication for hyperthyroidism, it may well turn out that the patient suffers from a TA or a TMNG disorder [14]. A thyroid gland with TMNG may function normally as a whole, but nodules may be overactive and other areas may be suppressed.

Figure 2.2: The CAPTUS 4000e detector system (Capintec, Inc.) [15].

Prior to the diagnostic procedure (and during the radioiodine therapy), the patient has followed a protocol that restrains iodine intake to avoid interfering with iodine uptake in the thyroid gland and thus the RAIU value. For the uptake measurement, a trace amount of radioiodine, either in the form of a capsule or a liquid solution in a test tube, is premeasured before administrated orally to the patient. The pre-measurement is used as a reference. The measurement of iodine in the patient's thyroid gland will thus be in relation to the reference value and corrected for radioactive decay. For the reference measurement, the capsule or test tube is placed in a plastic cylindrical phantom that imitates a neck in order to obtain a realistic geometry. The CAPTUS 4000e detector system (Capintec, Inc.), (see Figure 2.2) consisting of a NaI(Tl) crystal detector (thallium-activated sodium iodide) with a photomultiplier tube, is placed vertically above the phantom. The detector is equipped with a lead-shielded collimator tube, which has a pointer rod that indicates the center of the detector as well as the distance between the detector surface and the phantom surface [16], see Figure 2.3. The detector-to-surface distance is set to be 26 cm. The position of the detector is directly above the capsule and is determined visually using the pointer rod as a guide. An energy spectrum of ^{131}I (see Figure 2.4) is collected during a sample time of normally 300-600 seconds, corresponding to an administrated activity of 0.1-0.2 MBq. The number of pulses are determined within a region of interest (ROI) of $\pm 10\%$ from the center of the full energy peak at 365 keV, completely encompassing the full energy peak of ^{131}I [5, 16]. A background measurement, with the same measurement time and ROI, but without radioactivity in the neck phantom, is also required.

Five days after the performance of the pre-measurement and the administration of radioiodine, the RAIU in the patient's thyroid gland is measured (if the circumstances are changed, the patient measurement can be performed within eight days and still be valid). The patient lies down and the medical physicist visually and physically estimates the position of the thyroid gland, without the assistance of an endocrinologist. The detector is centered over the estimated thyroid gland position. The uptake measurement is performed according to the same protocol as the reference measurement five days earlier. The measurements are supplemented by a background measurement. The uptake measurement system generates an RAIU value expressed as a percentage compared to the reference measurement. The RAIU value is calculated as follows

$$RAIU = \frac{P - T}{C - B} \cdot 100, \tag{2.1}$$

where P is the count rate from the patient's neck 5 days after radioiodine ingestion, T is the background count rate on the same day as the patient measurement. C is the reference count rate, measured with the capsule or test tube and neck phantom, and B is the background count rate related to the reference count rate. The data is automatically decay corrected by the uptake measurement system [16].

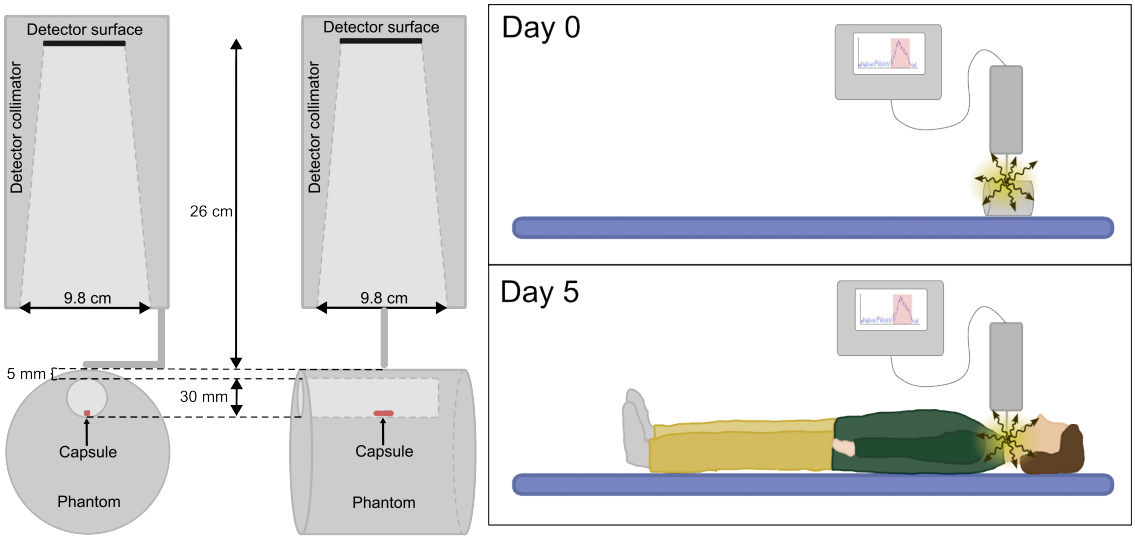

Figure 2.3: Left: Setup for the reference measurement with the uptake measurement system, with front view and side view. The detector-to-surface distance is 26 cm and the diameter of the detector opening is 9.8 cm. The hole diameter in the phantom is 30 mm and the thickness of the plexiglass on the top of the hole of the phantom is 5 mm. The illustration is with a radioiodine capsule. Right: Setup for the reference measurement (day 0) and for the patient measurement (day 5).

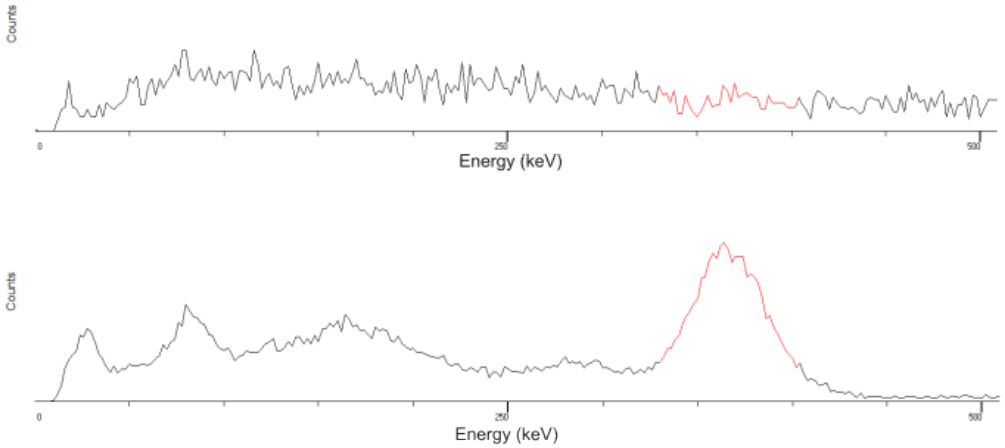

Figure 2.4: Example of spectra extracted from the uptake measurement system. The upper spectrum is with only background and the lower spectrum is with 0.1 MBq of radioiodine centered in the detector FOV. Pulses in the ROI (red in figure) are determined for background (upper diagram) and a combination of background and signal (lower diagram). The acquisition time was 300 seconds. Note that the y-axis is not the same in the two spectra.

2.3.1.1 Quality Assurance of Uptake Measurement System

Quality assurance (QA) tests of the Captus 4000e are performed before all patient measurements. The QA test includes Auto Calibration, Constancy Test and Chi-Square Test. The tests are performed with calibrated ^{137}Cs and ^{152}Eu standard sources. The calibrated activities were 18.5 kBq in 2017, for each source. The sources are placed, one at a time, in a rod source holder inside the collimator tube of the detector. The ^{137}Cs source is used to determine the Full Width at Half Maximum (FWHM) which is correlated to the resolution of the detector. Due to the user manual, the FWHM should be lower than 9.5% for the system to be considered successful. The ^{152}Eu source emits multiple gamma rays with energies between 41 and 1408 keV, which are used for the energy calibration of the system. The constancy test, using the ^{137}Cs source, determines the deviation between the measured and decay corrected calculated activity of the source. The deviation is accepted if the value is below 7.3%. In the end, a Chi-Square test, also using the ^{137}Cs source, is performed to determine how well the observed standard deviation conforms to the expected standard deviation of the system. The Chi-Square value should be between 3.33 and 16.9 for 95% of the time for it to pass. All levels for passed are according to the Captus user manual [16].

2.3.2 Estimation of Thyroid Gland Volume

The thyroid volume may be estimated in various ways: Ultrasound, computed tomography (CT), magnetic resonance imaging (MRI), planar scintigraphy (PS), single photon emission computed tomography (SPECT), physical palpation, or as a combination of these methods [4, 17, 18]. A nuclear scintigraphic method, based on radioactive uptake, i.e. PS and SPECT, reflects essentially the hyperactive thyroid gland volume and thus the volume to be treated. In contrast, the other mentioned methods predominantly shows the physical anatomy of the thyroid gland.

2.3.2.1 Planar Scintigraphy

The most common radioactive substance used for planar scintigraphy is ^{99m}Tc pertechnetate ($^{99m}TcO_4^-$), which is a pharmacologic mimic of iodine [14]. ^{99m}Tc has a half-life of 6.01 hours and emits 142.7 keV γ-rays [5]. This energy is within the energy range of photons that are suitable for the most common scintigraphic scanning methods using a gamma camera. In addition, the effective dose to the patient is minimized due to the short effective half-life of ^{99m}Tc. The uptake of technetium pertechnetate and thus the thyroid gland appearance on the scintigraphic image of ^{99m}Tc generally differ between the hyperthyroidism disorders. As can be seen in Figure 2.5, a healthy thyroid gland has an even distribution of technetium in the gland, with no hot spots or other intense uptake. Graves' disease also appears uniform but with a higher uptake of technetium throughout the gland and a suppressed background uptake, indicating a higher production of thyroid hormones (T3, T4). The disorders TA and TMNG have one or more nodules, which are hyperactive, and thus hotspots in the scintigrapic images can be seen. The anatomy of the thyroid gland can differ a lot, especially with TMNG, and the hotspots can be difficult to distinguish.

Once the patient has completed the uptake measurement, he or she is sent for PS imaging of the thyroid gland at the gamma camera NM/CT 870 DR (GE Medical Systems), see Figure 2.6. The acquisition parameters and gamma camera setup can be seen in Appendix A. Approximately 100 MBq of ^{99m}Tc-pertechnetate is intravenously injected to the patient. The scintigraphic scan is started 15 minutes after the injection, where the maximal accumulation occurs approximately 20

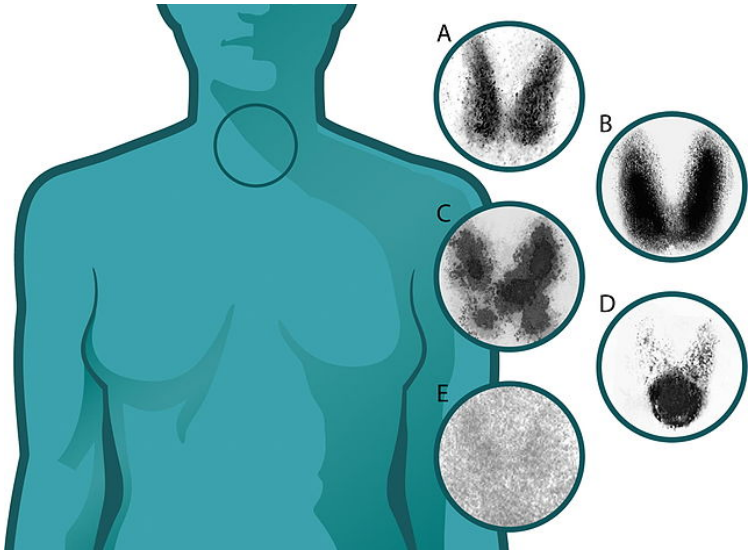

Figure 2.5: Planar scintigraphic images of the thyroid gland, with ^{99m}Tc pertechnetate. Thyroid gland with A) normal function, B) Graves' disease, C) toxic multinodular goitre, D) toxic adenoma and E) thyroiditis [19].

minutes after the injection [7]. In the gamma camera, the patient lies in supine position with the head first. Before the scan is started, it is confirmed that the thyroid gland and salivary glands are within the field of view (FOV).

2.3.2.2 Volume Estimation from Planar Scintigraphic Image

From the PS image, the active volume of the thyroid gland is estimated using a locally developed program in the Xeleris software (GE Medical Systems). This program reads the data from the PS image and allows the operator to create a ROI. The window settings are manually modified by the medical physicist so that the background in the image disappears sufficiently without changing the shape of the thyroid gland. The window settings in this case refers to the upper and lower limit of pixel values.

The user creates the ROI by freehand drawing in the image. How the ROI is drawn is described in the internal manual as follows: "Draw slightly inside the spiky outer contour". An example of a ROI can be seen in Figure 2.6. Up to three ROIs can be drawn, and usually the two lobes are drawn with one ROI each. If the shape of the thyroid gland is complex, a large ROI may be drawn for the entire volume. Consequently, the estimation of the volume is operator-dependent. The program determines the volume of each lobe based only on the area of the ROI. The volume V_{Lobe_x} of lobe x is calculated by using the Himanka-Larsson Formula [20]. This formula shows the linear correlation between the thyroid volume and the area of the frontal silhouette of the thyroid gland, based on *ex vivo* measurents. The formula is as follows

$$V_{\text{Lobe}_x} = 0.33 \cdot (\sqrt{A_{\text{ROI}_x}})^3 \tag{2.2}$$

where A_{ROI_x} is the area of the ROI over lobe x.

There are additional methods that can be used for estimation of the volume from a PS image. Those are based on a model that assumes the thyroid lobe to have a shape of an ellipsoid and the volume of the ellipsoid may be approximated based on a planar image [21]. In addition, the ROI that illustrates the area of the lobe could be determined by either manual or automatic segmentation, with the latter being operator-independent. Still, an assumption is made on the lobe thickness. The lobe thickness cannot be estimated from a side view PS scan, because the two lobes partly do overlap each other. Automatic segmentation can also be applied on SPECT images, where no assumption for the anatomy of the thyroid gland needs to be taken.

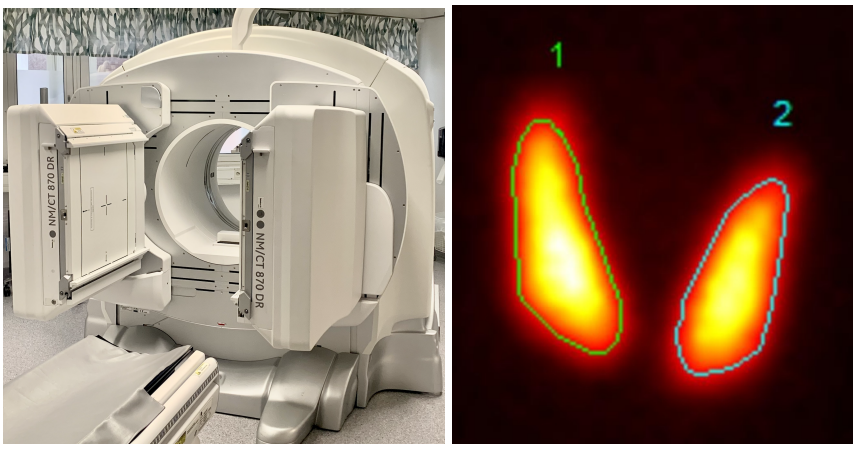

Figure 2.6: Left: Gamma camera of model NM/CT 870 DR (GE Healthcare). Right: Example of ROI drawn by freehand on PS image.

2.3.3 Radioiodine Therapy

If the physician recommends that the patient should receive radioiodine therapy, the prescribed absorbed dose depends on the diagnosis. The National Health Care Program for Hyperthyroidism in Sweden [2] recommends a target dose between 120 and 200 Gy for GD, if the goal is to achieve hypothyroidism. The recommendations for TA and TMNG are 300 Gy and 150-200Gy, respectively. At HSH, the target doses are set to be 120 Gy for GD, 300 Gy for TA and 150 Gy for TMNG.

2.3.3.1 Calculation of Activity to Reach the Target Dose

The mean absorbed dose per activity to the thyroid gland is calculated using the Marinelli formula [22], as

$$\frac{D}{A} = 0.043 \cdot \frac{U_0\, T_{eff}}{m} \tag{2.3}$$

where D is the target dose in Gy and A is the administered activity in MBq. U_0 is the extrapolated initial uptake of iodine in the thyroid gland at time zero given in percent, T_{eff} is the effective half-life of the radioiodine in the body given in days, 0.043 is a constant and m is the active thyroid mass in grams. The parameters U_0 and T_{eff} can be determined from multiple measurements, but Jönsson

et al [23] found a significant linear relationship that requires only a single uptake measurement. The relationship is as follows

$$U_0\, T_{eff} = k_t\, U_t, \tag{2.4}$$

where k_t is a linear coefficient depending on the time t in days of the uptake measurement and U_t is the measured RAIU value in percent at the same time t. The linear relationship is significant when the uptake measurement is performed between three and eight days after administration of radioiodine [4, 23]. The mean absorbed dose per activity to the thyroid gland is thus

$$\frac{D}{A} = 0.043 \cdot \frac{k_t\, U_t}{V}, \tag{2.5}$$

where also the mass m in g is converted to volume V in ml by the assumption of water density of 1 g/ml. At HSH, the patient measurement is performed five days after the reference measurement, and thus $k_t = 6.76$ [23]. To summarize, the administered activity of radioiodine to the patient does depend on the target dose prescribed to the patient, the RAIU value and the estimated active volume of the thyroid gland. This formula is used to determine the activity of the radioiodine to be administered to the patient, as follows

$$A = \frac{D}{0.043} \cdot \frac{V}{k_t U_t}. \tag{2.6}$$

2.3.4 Absorbed and Effective Doses from the Theragnostic Procedure

The absorbed doses to the thyroid gland and the effective doses from the radioiodine uptake measurement, the scintigraphic scan with technetium pertechnetate and the radioiodine therapy are listed in Table 2.1.

Table 2.1: Effective doses from uptake mesurement with radioiodine, from scintigraphic scan with technetium pertechnetate and from radioiodine therapy. The effective doses correlated to the activities used to diagnoose hyperthyroidism at HSH and an example of therapy activity. The effective doses are collected from the Swedish Radiation Safety Authority dose catalogue [24].

	Uptake measurement	**Scintigraphic scan**	**Radioiodine therapy**
Radiopharmaceutical	Sodium iodide ^{131}I	Technetium pertechnetate ^{99m}Tc	Sodium iodide ^{131}I
Activity (MBq)	0.1	100	600
Absorbed dose to thyroid gland (mGy)	58	2.2	348 000
Effective dose (mSv)	2.9	1.3	-

2.4 Factors Affecting the Therapeutic Absorbed Dose to the Thyroid Gland

There are many factors that may influence the actual absorbed target dose versus the prescribed target dose to the thyroid gland, see Figure 2.7. However, due to the project's limited time frame, not all factors were studied: some were studied in more detail whereas the others were just briefly discussed, although being of interest.

2.4.1 Radioiodine Uptake Measurement

For the uptake measurement, the following uncertainty factors were identified:

A1. Before the uptake measurement, the patient has received information about relevant medications. Some medications should not be taken as they affect iodine uptake [25]. However, if the patient does not comply, the iodine uptake at the time of the uptake measurement may differ from the uptake at the time of the administered therapy dose. However, compliance aspects were not treated in this project.

A2. A significant amount of the iodine administered is absorbed by the thyroid gland. However, the salivary glands may also absorb significant amounts of iodine, up to 13% [25, 26]. The salivary glands are relatively close to the thyroid gland, and ionizing radiation from radioiodine in the salivary glands may affect the RAIU value. However, this was not investigated in this project.

A3. The FOV, from the detector's point of view, increases when the detector-to-surface distance increases. This allows areas, such as salivary glands, to be within the FOV, see also A2. It is also known that the sensitivity of the detector decreases with increasing distance, due to the inverse square law. This is a matter of optimization and was therefore not investigated in this project.

A4. The reference measurement setup is designed to be as close as possible to the clinical measurement situation, but still fairly simple. The reference measurement of the radioiodine is performed by using the neck phantom, as can be seen in Figure 2.3. With this setup, an air gap is created between the radioactive source and the surface, when using a capsule or a small amount of liquid solution in a test tube. The diameter of the opening in the phantom is 30 mm. Therefore, with a small capsule or small amount of solution, the air gap is nearly 25 mm. This air gap is not created in a patient case, where the thyroid gland is surrounded by tissue. In addition, the phantom is not individualized for the patient, so the geometry of the phantom does not always match the geometry of the patient's neck. This was investigated to some extent.

A5. The reference measurement is carried out with a capsule or a test tube with liquid radioiodine solution, which is inserted into the phantom. The geometry of the capsule and the test tube is small and can be assumed to be point sources in relation to the area of the detector. In contrast, the patient's thyroid gland is not a point source and in extreme cases may lie outside the detector FOV. This was investigated to some extent.

A6. The sensitivity of the detector depends on the location of the radioactivity. In the case of reference measurement, where the capsule or test tube can be seen visually, the location is

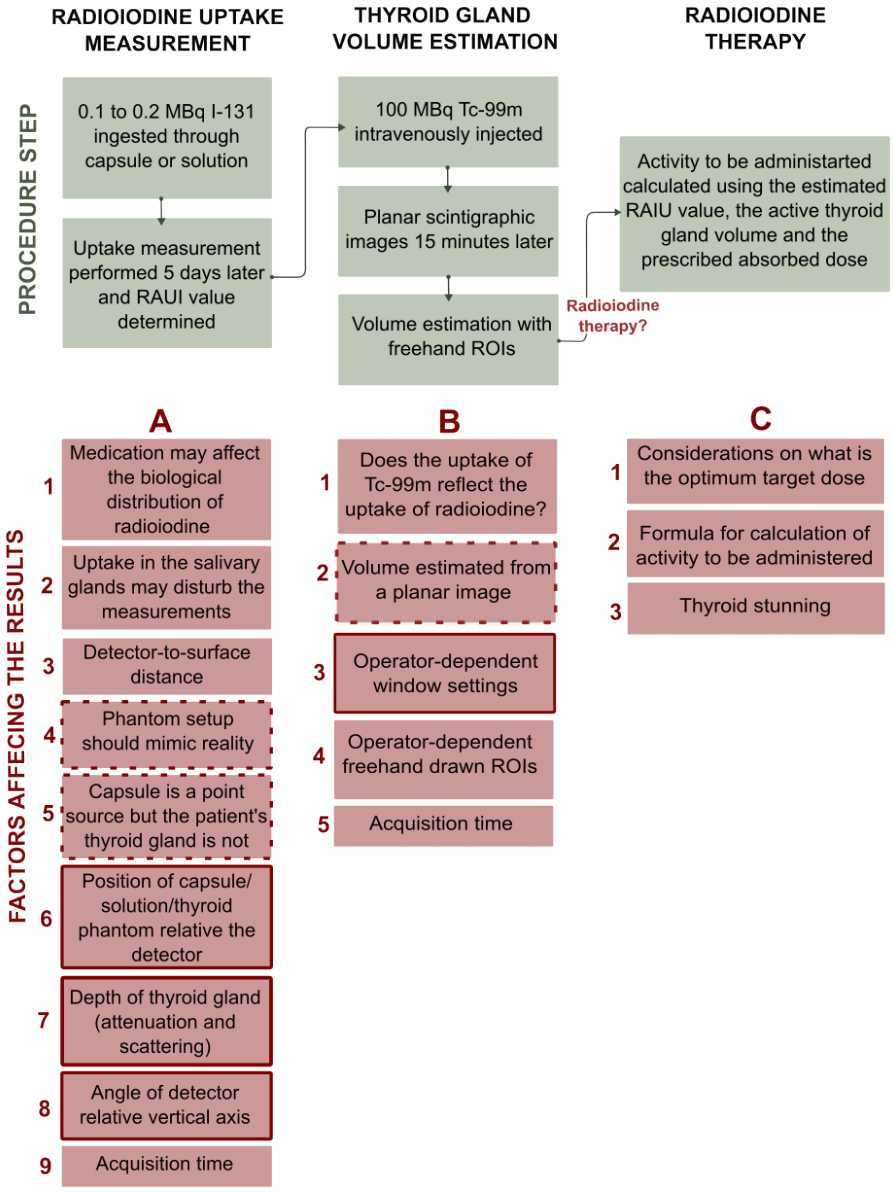

Figure 2.7: Schematic representation of the theragnostic steps for hyperthyroidism at the Nuclear Medicin Section at HSH (green boxes). The procedure is divided into uptake measurement, volume estimation and radioiodine therapy. The factors affecting the therapeutic absorbed dose to the thyroid gland are presented (red boxes). The factors are divided into subcategories A, B and C for uptake measurement, volume estimation and radioiodine therapy, respectively. Boxes outlined with solid and dashed lines were investigated and to some extent investigated, respectively, in this project. Boxes with no outlining were not investigated.

well known. In contrast, the exact location of the thyroid gland in the patient's neck is not known. The RAIU value may be affected if the center of the detector FOV deviates too much relative the location of the thyroid gland. This was investigated as part of the project. The investigation in this factor was used to answer A5 as well.

A7. The reference measurement is performed with the radioactivity at a well known depth in the plexiglass, and there is essentially no self-attenuation in the capsule or test tube. In the clinical situation, the depth from the skin surface to a nodule within the thyroid gland is not known. Therefore, there may exist some discrepancy between the measurement of the reference source at a fixed depth relative to a nodule at an unknown depth in the thyroid. Sometimes the difference in distance is negligible but at larger depth differences this may lead to deviations between the reference and patient measurement. This factor was investigated and is related to factor A4.

A8. The detector may be tilted to reach the thyroid gland region and if so, it depends on the operator how much. The detector FOV changes when the angle of the detector changes. Therefore, the position-dependent sensitivity is not the same as with a non-tilted detector. This was investigated in this project.

A9. The decay of radioactivity is a random process, and the uncertainty of the measurement is lower if the acquisition time is longer. However, the impact of the acquisition time on the RAIU value was not investigated in this project.

2.4.2 Thyroid Gland Volume Estimation

For the volume estimation of the thyroid gland, the following uncertainty factors were identified:

B1. The method for estimating the active thyroid volume is based on the assumption that the uptake of technetium pertechnetate in the scintigraphic images reflects the iodine uptake. If this is not the case, the volume estimated from the scintigraphic image with ^{99m}Tc is not the same volume that absorbs iodine and the estimated thyroid volume does not correspond to the treated volume. This uncertainty would exist for every patient case. However, this is a medical question and was not investigated in this project.

B2. The estimation of the active thyroid volume is based on a pure planar image without three-dimensional information. The volume is calculated from an assumption of a relationship between the area and a volume. The assumed relation used at HSH is seen in Equation 2.2. However, similar relationships, between area and volume, have been published, and the one chosen is decided by the individual clinic. This was investigated to some extent.

B3. The adjustment of the window settings on the PS image is subjective and may influence the appearance of the thyroid gland. If the upper level is lowered, the thyroid gland appears larger. If, on the other hand, the lower level is raised, the thyroid gland appears smaller. In addition, the intensity gradient is adjusted from the center to the edge of the thyroid gland. The operator-dependent window settings were investigated in this project.

B4. The area of the thyroid gland is drawn by freehand, based on the selected window settings. When the operator draws around the thyroid gland, he or she follows an intensity gradient and it is assumed that the same pixel value level is used for the entire area. The area drawn is

therefore highly dependent on the selected window settings. In addition, it is highly dependent on the operator which intensity is selected. This factor is linked to factor B3 but was not investigated in this project.

B5. The appearance of the thyroid gland depends on the acquisition time. The image quality and the statistic uncertainty improves with an increasing acquisition time. However, the impact of the acquisition time was not investigated in this project.

2.4.3 Other Influencing Factors

The uncertainty factors directly related to the therapeutic absorbed dose to the thyroid gland was not investigated in this project because of the medical aspects. Identified factors are:

C1. The National Care Program for Hyperthyroidism recommends an interval for the target dose for each type of diagnosis [2], and thus, the prescribed absorbed dose for the thyroid gland may vary between clinics. In addition, from a global point of view, it is not clear whether the goal is to bring the thyroid gland into underfunction (hypothyroidism) or normal function (euthyroidism) [27]. This may depend on the diagnosis and the future holds for the patient.

C2. The Marinelli formula, used for calculation of the radioactivity to administrate to the patient is based on measurements from about 70 years ago. There may be uncertainties in this formula originating from the uncertainties in the measurement methods used to develop it.

C3. Thyroid stunning may reduce the effect of the radioiodine therapy. Thyroid stunning is when the thyroid gland does not retain or absorb the radioiodine for therapy for a period of time after the administration of the trace amount of iodine for the uptake measurements [6].

3 Materials and Method

3.1 Production of Phantoms

3.1.1 Phantom Structure

An already existing thyroid phantom design, created by Jessen et al [28], was used for this study. This phantom was originally based on a digital phantom from the XCAT population which, in turn, consists of detailed anatomical structures of organs. These structures are based on anatomical datasets from the National Library of Medicine and patient datasets [29].

The 3D thyroid phantom by Jessen et al was created hollow with an added grid structure. The purpose of the grid structure was to create the possibility for radioactivity concentration differences within the phantom to reflect nodules in the thyroid gland. An empty phantom, without the grid structure, was also created to be able to determine the total volume of the phantom. The purpose Jessen et al had of the phantoms, were to create watertight phantoms to be filled with radioactive solutions. In addition, the phantoms should be reusable. The phantom was therefore equipped with a filling hole and a screw cap on top of each lobe. The phantom had a threaded hole below the "isthmus" part in order to be able to attach the phantom to e.g. a cylinder representing the patient neck [28].

The described phantom's grid structure only allowed a single concentration ratio between the volume with and without the grid structure. Therefore, the design with empty phantoms, i.e. without any grid structure was used in this study. The original phantom was recreated in the software Materialise Magics (Materialise) but also two larger sized phantom were made. These empty phantoms were used to reflect the active thyroid volume in GD. An additional phantom was created to simulate TA and TMNG. This phantom had the larger volume in order to reflect the generally larger thyroid glands in TMNG. Four extra volumes were also created inside the phantom, each fillable through narrow channels. These holes were not equipped with a screw cap, but were enclosed with quick drying silicone (illbruck, FA165) at the time of measurements. Photos of two of the phantoms (A3 and B) can be seen in Figure 3.1. The empty phantoms symbolizing GD patients were labeled A2, A3 and A4, with increasing volume, respectively. The phantom reflecting TA/TMNG was labeled B. Phantom model A4 and B were identical except for the extra volumes within phantom B. The lobes of the phantoms were labeled R (right) and L (left), corresponding to the orientation of the patient. In addition, the extra volumes within phantom B were labeled R1, R2 and L1, L2, respectively. In total, there were four phantoms created.

3.1.2 Phantom Printing

The thyroid phantoms were produced at 3D-centrum (Lund University, Sweden). A Form 3+ SLA printer (Formlabs) was used for phantom printing. The printing process took place in the liquid material Resin Clear V4 which was irradiated with a laser, creating a watertight object. The printing time per phantom was about seven hours, depending on the size of the phantom. The printed phantoms were cleaned with isopropanol in a Form Wash (Formlabs) to remove material residues and avoid clogging of the filling hole. Finally, they were hardened with UV light in a Form Cure (Formlabs). Hardened resin has a density of 1.2 g/cm^3, slightly higher than the density of water. However, Jessen et al found no effects on scintigraphic images with attenuation correction [28].

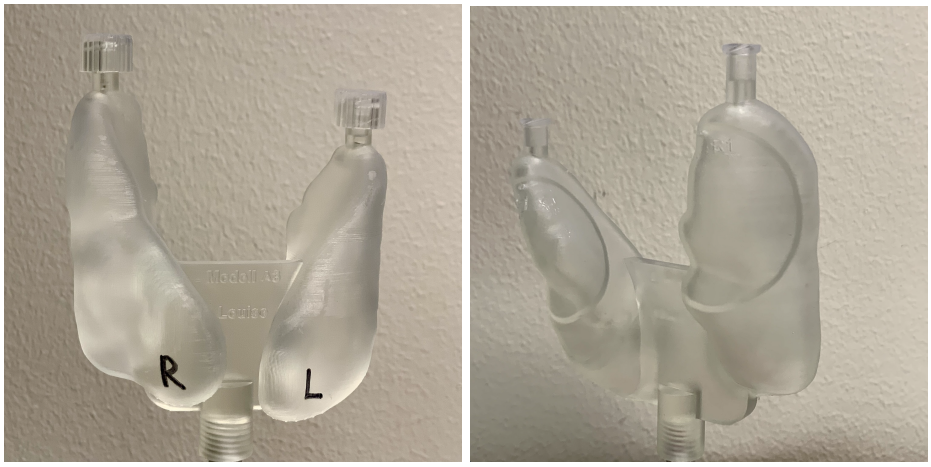

Figure 3.1: Thyroid phantoms, model A3 (left) and model B (right). The back of phantom B is shown to visualize two out of four hotspots. Note that phantom A3 has the screw caps on, whereas phantom B not.

The hollow volume, V, of a phantom was calculated from the mass difference of the empty phantom and when it was completely water filled. The mass was converted to volume by approximate the density of water to be 1 g/cm^3. The lobes were filled with water using a syringe and a needle. The filling process was performed slowly as not to create air bubbles. The goal was to repeat this process a few times to ensure that the volume of the phantom was determined with as high accuracy as possible. However, this was only possible for phantom A2 and B. Phantom A3 was filled with radioiodine before the volume process was repeated (and due to the long half-life of ^{131}I, the phantom was not used again) and phantom A4 did break by an accident. For phantom A2 and B, the process was repeated three times. Between each occasion, the phantom completely dried. As the lobes and hotspots of the thyroid phantom were filled separately, this process was performed for each lobe and each hotspot.

3.1.3 Thyroid Phantom Volumes

The measured volume of all used phantoms is seen in Table 3.1. For all phantoms, the right lobe had a larger volume than the left lobe. The total volume, for each phantom, ranged from 18.8 to 37.0 ml. This volume range includes most normally functioning thyroid glands as well as a slightly enlarged thyroid gland. However, glands with even larger volumes were subsequently not dealt with in the present study. Model B and model A4 have identical form, but model B has added walls for the hotspots. Thus, the total volume given for model B is the same as for model A4 (37.0 ml). The total summarized volume for the fillable volumes within model B is 34.2. However, this volume is not used as a reference because the small volume of the wall is not distinguished in the scintigraphic images but belongs to the total volume.

Table 3.1: The hollow volume in ml of the phantom models A2, A3, A4 and B. The represented diagnoses are also listed. For phantom model B, the volumes of each hotspot (L1, L2, R1, R2) are shown. The total volume represents the two lobes together. * The summarized fillable volume of phantom model B. ** The total volume of phantom model B.

Phantom model	**A2**	**A3**	**A4**	**B**
Diagnosis	**GD**	**GD**	**GD**	**TA/TMNG**
Left Lobe	8.2	12.3	16.2	4.0
Right Lobe	10.5	15.7	20.8	10.6
L1	-	-	-	4.5
L2	-	-	-	6.4
R1	-	-	-	4.7
R2	-	-	-	4.1
Total volume (ml)	18.8	28.1	37.0	(34.2)* 37.0**

3.2 Radioiodine Uptake Measurements

3.2.1 Source Position Dependence

The detector position relative to the thyroid gland position may possibly affect the uptake value because of an altered detector FOV. The position dependence was investigated, with measurements on a radioiodine capsule, on a test tube with liquid solution of radioiodine and on a thyroid phantom (A3) filled with a liquid solution of radioiodine. The activity of the sources were in the same order as the activity administered to the patient at a radioiodine uptake measurement (0.1 MBq). The activity in the thyroid gland of the patient by the time of measurement five days after the administration is lower than this. This may imply lower uncertainties and better statistics in the experimental experiments compared to the patient measurements. Prior to the measurements, a QA (see Section 2.3.1) as well as a background measurement, without any radioactive sources, were performed.

The source (i.e. the capsule, test tube or thyroid phantom) was placed under a plexiglass plate with the thickness of nine millimeters. The plexiglass was used to simulate overlapping tissue in the neck, which is 5-10 mm thick. The available 9 mm thick plexiglass plate was assumed to reflect the tissue in the patient's neck well. For the first measurement, the source was centered under the detector with help of the pointer rod. The following measurements were performed with the source in different positions. During and between the measurements, the detector position was fixed while the source position was varied using a matrix, placed under the source and the plexiglass plate. The matrix can be seen in Appendix B. The matrix elements were 1x1 cm^2 and named X1 to X15, and Y1 to Y15, respectively. The source was centered on the dot of each element moved by 1 cm at the time, up to 14 cm. Measurements were performed in horizontal (X), vertical (Y) and diagonal direction as to indicate the source position dependent sensitivity of the detector. The first measurements were performed with the capsule, with the acquisition time 240 seconds per position. Afterwards, the acquisition time was increased to 300 seconds for the test tube and the phantom, to decrease the statistically fluctuations. The counts per second (CPS) value was documented from each test measurement. The capsule had the dimensions 15x5x5 mm^3. The liquid solution of radioiodine in the test tube had the shape of an ellipsoid, with an estimated dimension of 15x30 mm^2,

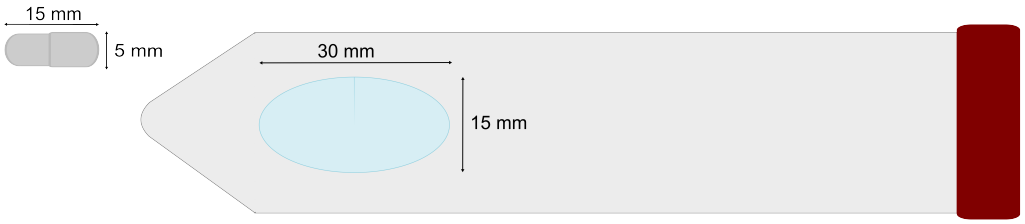

Figure 3.2: Illustration of the radioiodine capsule (left) and the test tube with liquid solution of radioiodine (right). The illustration is seen from above. The estimated dimensions are presented in the image.

seen from above. Illustrations of the capsule and test tube can be seen in Figure 3.2 and the third test object, the thyroid phantom, is described in Section 3.1.

3.2.2 Source Depth Dependence

There is a natural variation in depth from the skin to different parts of the thyroid gland. This may affect the dependence of detected pulses, due to attenuation and scatter of the photons. The depth dependence was investigated using various thicknesses of plexiglass plates. The measurements were performed with a radioiodine capsule, a test tube with a liquid radioiodine solution (see Figure 3.2) and a thyroid phantom (model A3) with a liquid solution of radioiodine (see Section 3.1). The activity of the sources was in the same order as the administered activity to the patient at radioiodine uptake measurements (0.1 MBq).

Prior to the experimental measurements, a background measurement without radioactive sources present was also performed. The CPS value was determined for each measurement. The source used was centered under the detector with the pointer rod as guidance. The first measurement was performed with no plexiglass between the radioactive source and the detector. The absorber measurements were performed with an increment of three millimeter thick plexiglass (which was available at the clinic) compared with the previous measurement. The maximum absorber thickness was 30 mm, including both tissue and thyroid gland. The setup was as in Figure 2.3, but with flat plexiglass plates instead of the neck phantom. The detector-to-surface distance was fixed to 26 cm, but the detector-to-source distance increased with increasing plexiglass thickness. Due to limited availability of plexiglass, two different types of plexiglass materials were used. However, this was recognized after all measurements were performed. The acquisition time, at each absorber thickness, was 300 seconds for the three source types.

3.2.3 Detector Angle Dependence

The angle of the detector may be changed when measuring on a patient in the clinical situation. This may affect the measurements because of the changed area seen by the detector. This was investigated by varying the angle of the detector, see Figure 3.3. The measurements were performed with a test tube (see Figure 3.2) and a thyroid phantom (model A3) (see Section 3.1) containing a liquid radioiodine solution. The activity of the sources were in the same order as the administered activity to the patient at radioiodine uptake measurements (0.1 MBq). No capsule measurements

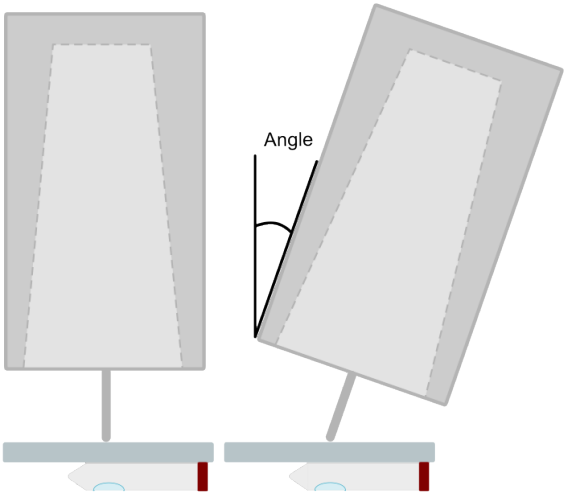

Figure 3.3: The setup for uptake measurements at perpendicular incidence (left) and with a tilted detector (right). The used test tube, with an approximately ellipsoid-liquid radioiodine solution, is also illustrated.

were performed because there were no longer any available at the clinic. During the measurements, either source was placed under a nine millimeter thick plexiglass plate. The detector angle varied from 0° to 40° and with an interval of 5° and the angle was measured using an digital angle meter. For each angle, the detector was adjusted to have the source centered under the detector, using the pointer rod as guidance. The acquisition time was 300 seconds per angle.

3.2.4 Air Gap Dependence

At the reference measurement, there is an air gap created between the radioactive source and the surface in the neck phantom, see Figure 2.3. However, this is not the case when measuring on a patient. Measurements were performed with and without an air gap in the previously described neck phantom (see Figure 2.3). A liquid solution of radioiodine was used, in the tip of a syringe. The activity of the solution was in the same order as the administered activity to the patient at radioiodine uptake measurements (0.1 MBq). When the syringe was placed on the bottom of the cylindrical opening, an air gap was created, but when uplifted by use of tissue paper, no air gap was created. Five measurements with each setup were performed with an acquisition time of 120 seconds, to minimize the effects of statistical fluctuations.

3.3 Thyroid Phantom Estimation using Scintigraphic Methods

3.3.1 Phantom Preparations

The 3D-printed thyroid phantoms were used for the scintigraphic scans. As previously mentioned, phantom models A2, A3 and A4 represented GD and phantom model B represented a combination of TA and TMNG. A cylindrical phantom with a diameter of 11.8 cm, made of polyethylene terephthalate (PET) material, was used to represent the neck of a patient. The volume of the cylindrical

phantom was 2100 ml.

The thyroid phantom was filled with water in the same way as previously described and a small volume was left empty, for the technetium pertechnetate to fit. The technetium pertechnetate was prepared in syringes, one for each lobe and the activity was measured and documented. The technetium was then slowly injected to the water filled phantom with the syringe and needle. Because of the low activity administered to the phantom, the activity volume was very small, thus like a point source in the syringe. To ensure that the majority of the activity had been injected to the phantom and not stuck in the needle, the syringe was emptied and refilled repeatedly into the thyroid phantom with water. Afterwards, the rest of the activity in the syringe was measured in the activity meter to be able to know the actual injected activity.

The filling process of phantom model B did differ from that of phantom models A. Because of the small volumes in the hotspots, it was hard to see when the volume was completely filled with water. Also, it was easy for it to spill over. If this would have happened, the activity in the hotspot would not be as high as wanted. Thus, a branch solution was used, with a fixed activity concentration. In this way, spilling would not cause a difference in the amount of injected activity. The process was performed cautiously, and only a small amount of activity was in fact spilled and no contamination did occur. The small channels to the hotspots in the phantom was closed with silicone.

The thyroid phantom was attached to the lid of the cylindrical phantom so that the phantom was at a realistic depth, see Figure 3.4. The distance between thyroid phantom surface and the cylindrical

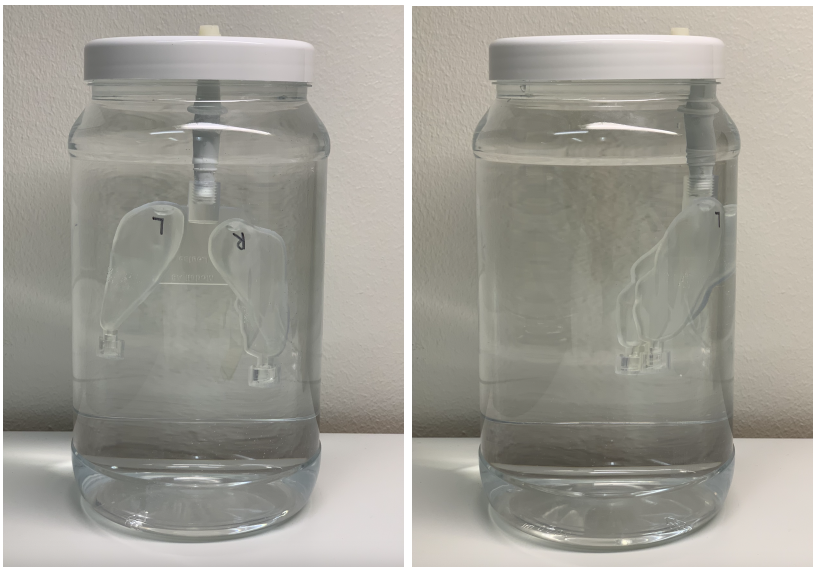

Figure 3.4: The total phantom used for the scintigraphic scans. A thyroid phantom of model A3 is placed inside the cylindrical phantom, representing the neck of a patient.

inside was not measured but visually approximated to be between 5-10 mm, depending on which phantom model that was used. Radioactive ^{99m}Tc was added to the cylindrical phantom to mimic the background activity in the neck of a patient. This was possible, because previously, a small hole was created in the lid of the cylindrical phantom and the hole was covered with water proof tape after the activity injection.

Various combinations of activity in the thyroid and cylindrical phantoms were achieved by having technetium in the thyroid phantoms to decay. Meanwhile, additional activity was injected to the cylindrical phantom through the small hole. In this way, the thyroid phantom activity decreased while the cylindrical phantom activity increased. The activities used are seen in Table 3.2. In phantom B, the hotspots were filled with five times as much activity as the rest of the thyroid phantom. The cylindrical phantom was filled with roughly 20 MBq. Additional 5-10 MBq was injected between the scans. The images extracted with these activities were visually assumed to reasonable reflect clinical cases.

Table 3.2: Total activity (MBq) and activity concentrations (MBq/ml) of technetium pertechnetate used for the thyroid phantom models A and B, as well as for the cylindrical phantom.

	Phantoms A	**Phantom B**
Thyroid Phantom Lobes	20 MBq	0.4 MBq/ml
Thyroid Phantom Hotspots	-	2 MBq/ml
Cylindrical phantom	20 MBq	20 MBq
Additional (cylindrical phantom)	5-10 MBq	5-10 MBq

3.3.2 Scintigraphic Scan with Gamma Camera

Scintigraphic scans of the complete phantoms were produced with the gamma camera NM/CT 870 DR (GE Healthcare), see Figure 2.6. Both a planar scintigraphic (PS) scan and a SPECT scan were acquired for each phantom. Essentially, the same acquisition parameters were used as for clinical thyroid scintigraphy. The acquisition time was however decreased by 50% to save time and instead, the activity in the phantoms was doubled to achieve the same number of counts in the images. The gamma camera settings and acquisition parameters can be seen in Appendix A. For the PS scan, the camera head was placed as near as possible to the phantom, and for the SPECT scan, the camera head was positioned automatically by the camera system implying different detector-to-source distances between the projections. In total for each phantom (A2, A3, A4, B) four PS scans and four SPECT scans were taken. As previously described, between the scans, activity decay occurred and additional activity was administered to the cylindrical phantom.

3.3.3 Pulse Count Ratios in Scintigraphic Images

For the evaluation of the scintigraphic images, it was of interest to know the ratio in pulse counts between the thyroid phantom and the background (cylindrical phantom). The average pulses per pixel was documented and was calculated as the total number of pulses within the ROI devided by the number of pixels within that ROI. The average pulse count ratio, CR, was defined as

$$CR = \frac{\text{average number of pulses per pixel in thyroid ROI}}{\text{average number of pulses per pixel in background ROI}}. \tag{3.1}$$

The ROI over the thyroid phantom image was drawn by using the original window settings and the ROI line followed the same color intensity (sharp red) around the thyroid phantom image, see Figure 3.5 for examples of ROIs. The rectangular ROI for the background was placed well outside of the thyroid phantom. To ensure this, the window settings were adjusted so the thyroid phantom edge could be seen clearly. For the SPECT images, the ROIs were drawn on the first projection (and not on the reconstructed image), to be comparable to the CR for the PS images. This procedure was also performed on clinical cases, to ensure that the ratios in the phantom images were realistic. In total, five patients per diagnosis (GD, TA, TMNG) were randomly selected.

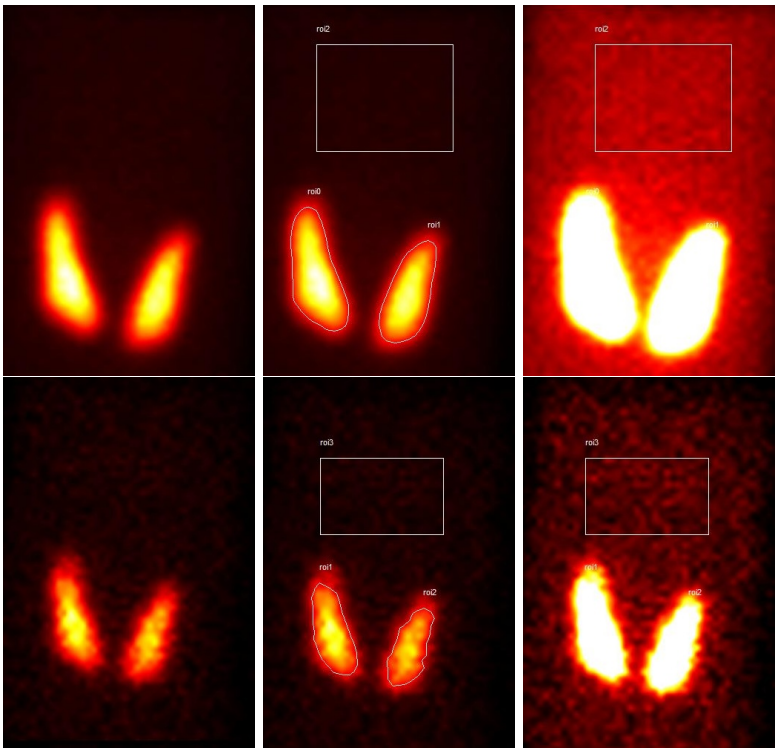

Figure 3.5: Scintigraphic images of thyroid phantoms. Upper row: PS images. Lower row: SPECT images (one projection without reconstruction). Left column: Image with original window settings and without any ROI. Middle column: Image with original window settings and ROI around the thyroid phantom lobes and of the background. Right column: Changed window settings (upper boundary was lowered) and ROI around the thyroid phantom lobes and of the background.

3.3.4 Thyroid Phantom Volume Estimation from Scintigraphic Scans

Three methods were used to estimate the volume of the thyroid phantoms based on the scintigraphic images. The first method is the same as that used at the clinic, i.e. freehand drawn ROIs in PS

images. The second and third methods are based on automatically segmented PS and SPECT images.

3.3.4.1 Estimated Thyroid Phantom Volumes from Freehand Drawn ROIs

Three experienced medical physicists (MP) at HSH drew ROIs in the images as if it was a clinical case, i.e., they followed the standard procedure for clinical images. The Xeleris (GE Medical Systems) software calculated the volume based on the area of the ROI, according to Equation 2.2. The procedure was repeated for each lobe in the phantom image and the volume for each lobe as well as the summarized volume were presented by the software. MP 1 and MP 2 repeated this procedure twice for every twelve phantom images, and MP 3 was not able to repeat the procedure. More trials would be more ideal to obtain better statistics. However, the MPs did have limited time to repeat the procedure. The results from the first drawing of phantom models A were presented to the MPs before they drew the second time, possibly influencing them to somewhat adjust their individual drawing methods. The MPS did draw on the images of phantom model B after the presentation and discussion of the results from Trial 1 of the phantom models A.

3.3.4.2 Estimated Thyroid Phantom Volumes from Automatic Segmentation

The volume of the thyroid phantoms were also estimated by using automatic image segmentation, on both the PS and the SPECT images. This was performed with a programming code, manually created in the programming language Python. For both PS and SPECT images, the code segmented pixels with a pixel value above a certain threshold value. Figure 3.6 shows an example of a segmented PS image. The threshold value was set by the operator. All pixels with values above this threshold were set to 1, and the rest to 0. The choice of threshold value thus affected the estimated phantom volume. Therefore, the threshold value was varied to be able to compare resulting volumes with the true phantom volume. Pixel and voxel sizes were inserted into the programming code, for PS and SPECT images, respectively.

The segmented area A_{seg}, for the PS images, was calculated with the following formula

$$A_{\text{seg}} = N_{\text{pixels}} \cdot A_{\text{pixel}}, \tag{3.2}$$

where N_{pixels} is the number of segmented pixels and A_{pixel} is the pixel size in mm^2. The estimated phantom volume of each lobe was calculated according to Equation 2.2. Unfortunately, the programming code could not separate the two lobes when calculating the number of segmented pixels. This was corrected for by dividing the segmented area by two. This was assumed to be approximately correct, by visually assessing the size of the segmented lobes to be the same size.

The volumes of the thyroid phantoms, based on the SPECT images, were estimated by summarizing the number of segmented voxels, instead of number of pixels. The segmented volume V_{seg} was then calculated with the following formula

$$V_{\text{seg}} = N_{\text{voxels}} \cdot V_{\text{voxel}}, \tag{3.3}$$

where N_{voxels} is the number of segmented voxels and V_{voxel} is the voxel size in mm^3.

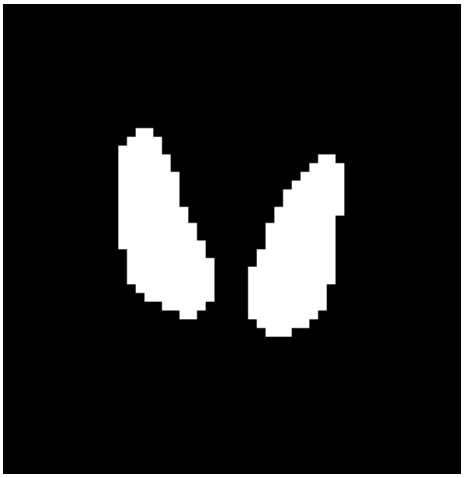

Figure 3.6: Example of a segmented PS image with a threshold value of 25%.

4 Results

4.1 Uptake Measurements

4.1.1 Source Position Dependence

The source position dependence is shown in Figure 4.1. The results from the three directions (X, Y and diagonal) did agree but with a small shift due to the not perfect centered source at the first measurement. Thus, the results shows the data acquired only from the X-direction positions. It is seen that the sensitivity of the detector was not 100% across the detector diameter. At the edge of the opening (marked as detector radius), the sensitivity was 92-95%, slightly depending on source type. Overall, the curve had the same shape for all sources, however, beyond the edge, the difference between the sources increased. The sensitivity for the capsule (the smallest source) decreased slowly immediately after the detector edge, but dropped faster after about 7 cm compared to the other sources. The phantom source, on the other hand, had a more slow drop and a higher sensitivity further away from the center compared to the other sources. The curve for the test tube was between the capsule and phantom sources. The decline per centimeter between 6 and 9 cm for the capsule, liquid solution and phantom was 26%, 24% and 19%, respectively.

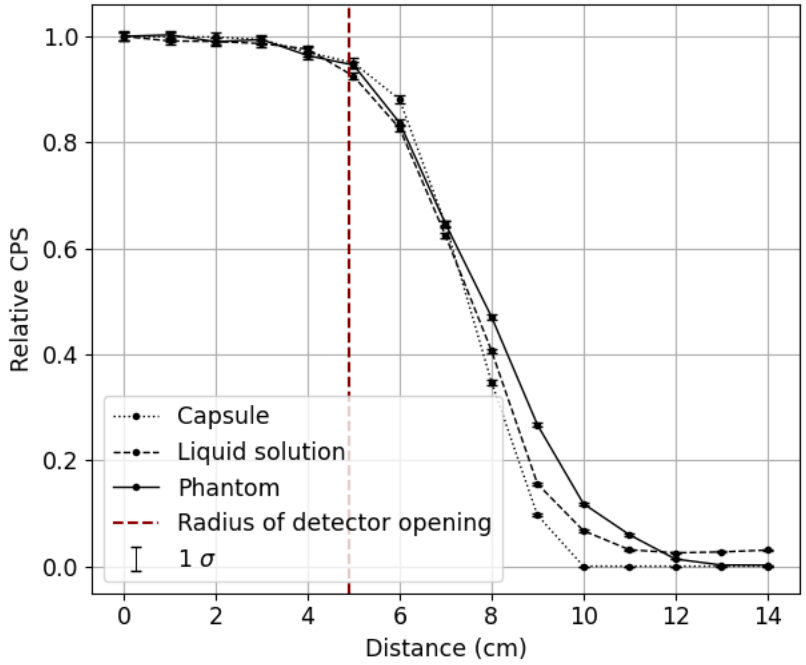

Figure 4.1: The sensitivity of the detector as function of the source position. The source types are a capsule, liquid solution in a test tube and a thyroid phantom (model A3). The vertical axis shows the counts per second (CPS) relative to CPS at x=0, for each studied source, respectively. The horizontal axis shows the distance in centimeters from the center of the detector FOV, i.e. at x=0. The detector radius is presented with a red dashed line. The vertical error bars shows one S.D.

4.1.2 Source Depth Dependence

The source depth dependence is shown in Figure 4.2. It is seen that the overall decline with depth for the sources is larger than the distance corrected theoretical attenuation. The theoretical attenuation does not include scatter detection. In addition, none of the source curves were straight, as the theoretical attenuation curve. Note that it was not only the thickness of plexiglas that changes. With increasing thickness, the detector-to-source distance increased, even though the detector-to-surface distance was constant.

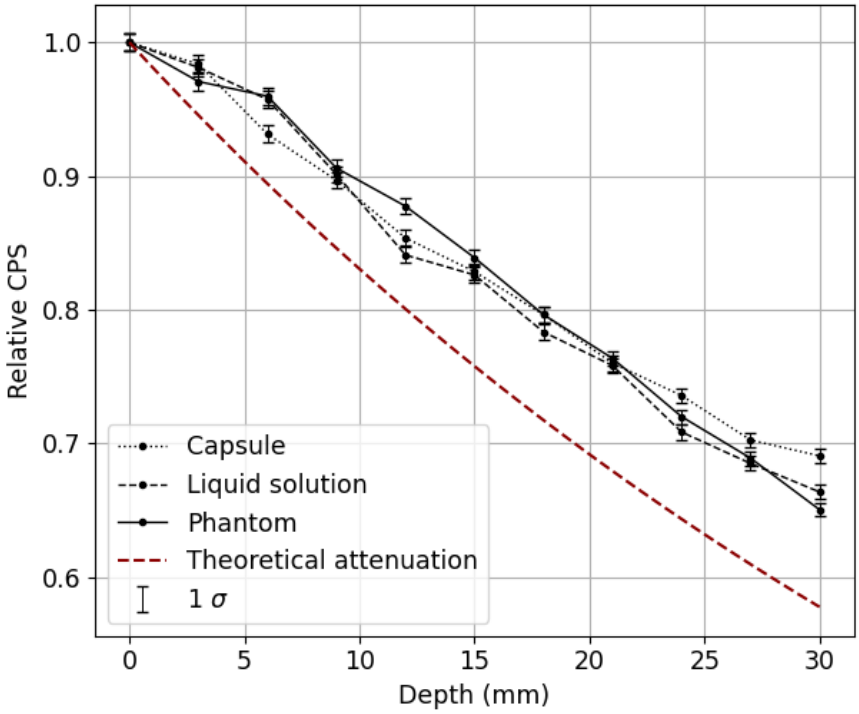

Figure 4.2: The sensitivity of the detector as function of the source depth. The source types are a capsule, liquid solution in a test tube and a thyroid phantom (model A3). The vertical axis shows the counts per second (CPS) relative to CPS at x=0 (no plexiglass), for each studied source, respectively. The horizontal axis shows the source depth in millimeters. The theoretical attenuation (red dahed line) shows the theoretically attenuation for plexiglass, water and tissue (attenuation factor 0.11 cm^2/g at 365 keV). The theoretically attenuation is distance corrected with the inverse square law. The vertical error bars shows one S.D. calculated from the counts in the measurement. Note that the vertical axis has a cut off.

4.1.3 Detector Angle Dependence

The detector angle dependence is seen in Figure 4.3. The detector sensitivity decreased when the angle increased, until angle 25°, where it started to increase. However, it was only a small change, where the maximum deviation from the 0° angle was 3.5%, which occurred at an angle of 15°.

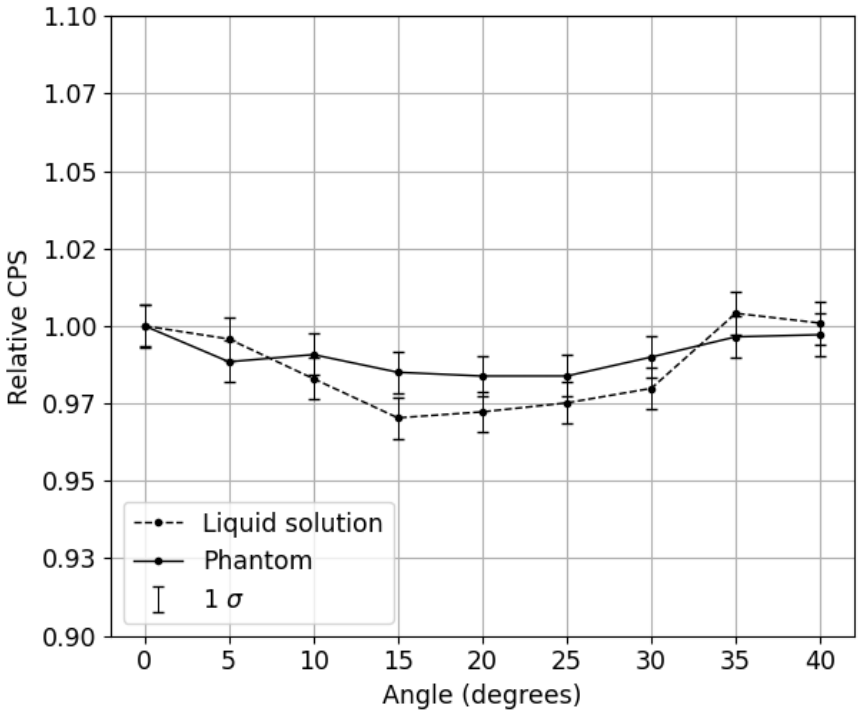

Figure 4.3: The sensitivity of the detector as function of the detector angle. The source types are a capsule, liquid solution in a test tube and a thyroid phantom (model A3). The vertical axis shows the counts per second (CPS) relative to CPS at X=0 (angle 0°). The horizontal axis shows the detector angle in degrees. The vertical error bars shows one S.D. Note that the vertical axis has a cut off.

4.1.4 Air Gap Dependence

The air gap dependence is seen in Table 4.1. The detector-to-source distance changes between the two types of setups (larger distance with air gap), but the detector-to-surface distance remained constant. Without any correction for the distance difference, the ratio between the number of counts without air gap and with air gap was 1.27 (27% deviation). With correction for the distance difference (with the inverse square law) the ratio was 1.06 (6% deviation). The distance difference was approximately 25 mm.

Table 4.1: The mean number of counts from five measurements with and without air gap in the neck phantom. The lower row is corrected for the extra distance with air gap, using the inverse square law. The acquisition time was 120 seconds per measurement. The deviation shows the ratio between the counts without air gap and with air gap. One S.D is applied to the results.

	Counts with air gap	**Counts without air gap**	**Deviation (%)**
Not corrected	1430 ± 40	1810 ± 40	27 ± 5
Corrected	1710 ± 40	1810 ± 40	6 ± 3

4.2 Thyroid Phantom Volume Estimation

4.2.1 Count ratio (CR) of gland to background ROIs

The count ratio (CR), between the thyroid and background, for five, randomly selected patients, per diagnosis (GD, TA, TMNG) are seen in Table 4.2. For this limited number of clinical cases, GD had the largest CR (26.3). Also, the smallest CR for GD was smaller than all CR for TA. TMNG showed a smaller range of CR values. Thus, GD seems to have a larger range than TA and TMNG.

Table 4.2: CR between thyroid and background in PS images for clinical cases.

GD	TA	TMNG
9.7	12.4	3.2
17.3	13.9	4.1
18.0	16.5	4.8
22.0	17.0	5.0
26.3	18.9	5.7

CR values for phantom measurements are seen in Table 4.3. The largest CR was 13.8 for phantom B with SPECT. The smallest CR was 4.2 for phantom A4 with PS. The largest CR was not as large as the largest CR for the clinical cases. For comparison, the correlated CRs between PS and SPECT was not exactly the same, as well as they were not between the phantom models.

Table 4.3: CR in PS and SPECT images for phantom measurements with phantom models A2, A3, A4 and B.

	A2				A3				A4				B			
PS	10.9	8.8	7.0	5.9	9.9	7.8	6.2	5.1	8.5	6.3	5.1	4.2	11.9	7.2	6.6	5.0
SPECT	12.1	9.0	7.5	6.4	10.9	8.3	6.9	6.0	10.0	7.3	6.0	4.8	13.8	10.3	6.9	6.0

4.2.2 Estimated Thyroid Phantom Volumes from Freehand Drawn ROIs

4.2.2.1 Phantom Models A

The window settings used by the medical physicists (MP) when drawing the ROI on the PS images of phantom models A are seen in Table 4.4. MP 1 and MP 3 used 100% for the upper limit, for all images, as specified in the method description. On the contrary, MP 2 used a window setting between 76% and 100% for the upper limit, and no change in the lower limit. For MP 1, the lower limit was between 3% and 17% for Trial 1. For Trial 2, MP 1 used all lower limits lower than those used in Trial 1. A similar comparison for MP 2 showed that this person slightly increased the upper limit for majority of the images in Trial 2. This comparison cannot be made for MP 3 with only one trial. In addition, MP 3 used an overall lower limit in all images compared to MP 1's Trial 1.

Table 4.4: Window settings used by the MPs when drawing ROIs in PS images of phantom models A. CR is shown for every measurement. The upper and lower levels show in percentage the limit chosen by the MPs, in relation to the maximal pixel value in each image. The MPs did draw twice (except MP 3), and this is shown as Trial 1 and Trial 2. * Upper limit not recorded.

	Trial		**A2**				**A3**				**A4**			
		CR →	**10.9**	**8.8**	**7.0**	**5.9**	**9.9**	**7.8**	**6.2**	**5.1**	**8.5**	**6.3**	**5.1**	**4.2**
MP 1	**1**	**Upper**	100	100	100	100	100	100	100	100	100	100	100	100
		Lower	3	6	9	10	8	9	12	12	8	11	14	17
	2	**Upper**	100	100	100	100	100	100	100	100	100	100	100	100
		Lower	2	4	5	5	4	5	5	6	8	4	6	6
MP 2	**1**	**Upper**	78	85	82	87	76	85	86	91	91	84	84	100
		Lower	0	0	0	0	0	0	0	0	0	0	0	0
	2	**Upper**	?*	89	91	92	93	95	92	91	86	90	85	89
		Lower	0	0	0	0	0	0	0	0	0	0	0	0
MP 3	**1**	**Upper**	100	100	100	100	100	100	100	100	100	100	100	100
		Lower	1	4	6	5	3	7	7	6	6	10	11	11
	2	**Upper**	-	-	-	-	-	-	-	-	-	-	-	-
		Lower	-	-	-	-	-	-	-	-	-	-	-	-

The volumes estimated based on the drawn ROIs by the MPs on the PS images of phantom models A are seen in Figure 4.4. Note that MP 3 did not perform a Trial 2. For Trial 1, it can be observed MP 1 and MP 3 overall drew similar volumes, meanwhile MP 2 drew larger volumes. The results show that MP 2 drew volumes larger than the true volume of the phantom (overall), and MP 1 and MP 3 drew volumes smaller than the true volume. For Trial 2, MP 1 drew larger volumes compared to Trial 1 which is the opposite to MP 2, who overall drew smaller volumes in Trail 2 compared to Trial 1. It is seen from the box plots that the spread in estimated volume, for each MP and trial, was relatively small except for the estimated volumes of phantom A4 by MP 2. Also, the spread increased with increasing phantom volume for MP 2, while this pattern could not be seen for MP 1. The deviation from the true volume presented in percentage is shown in Section 4.2.5 for all data.

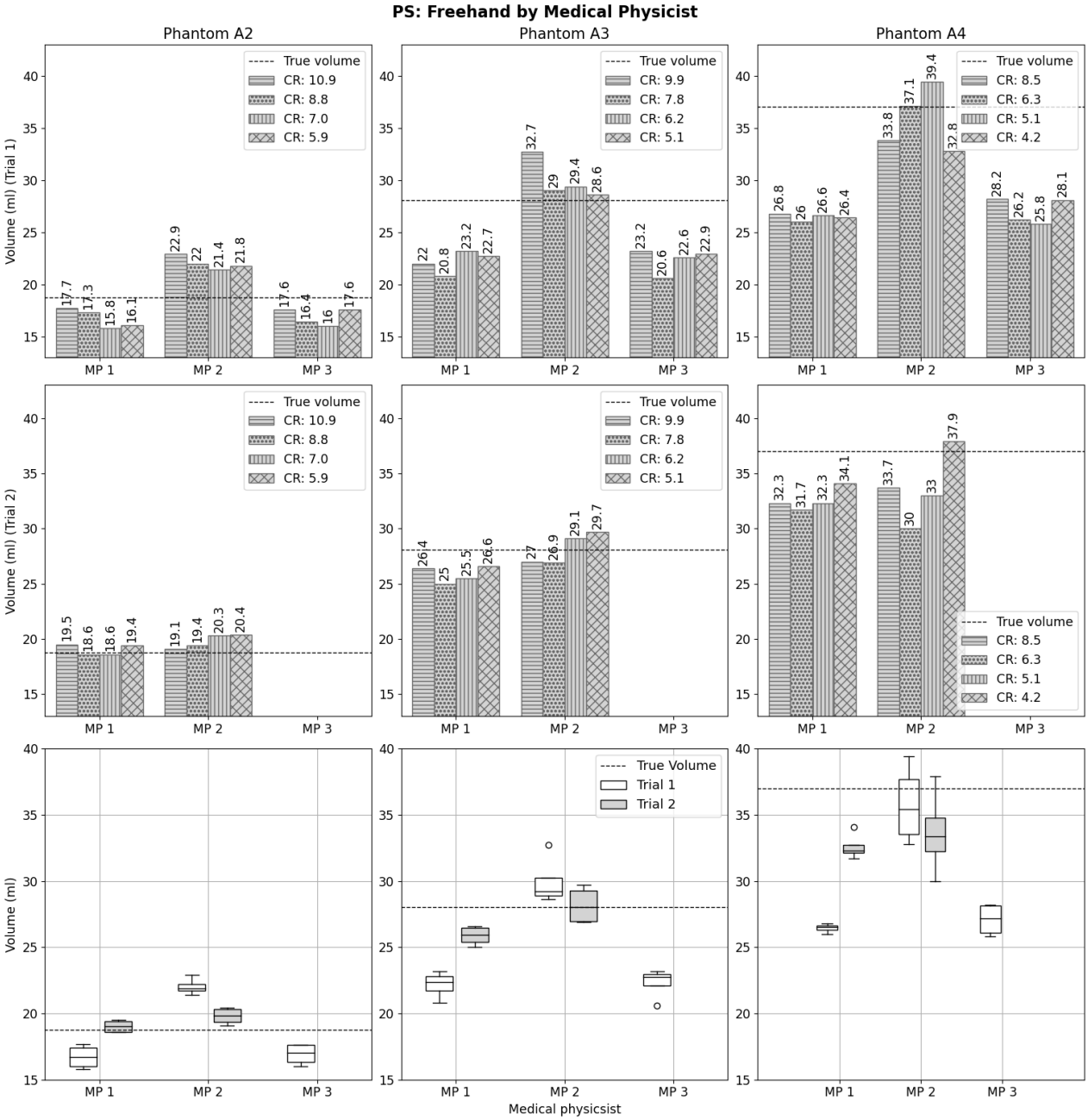

Figure 4.4: Phantom volumes estimated from ROIs, drawn by freehand on PS images, by three medical physicists (MP 1 - 3). The true volume for each phantom is indicated by the dashed line. The CR for each image is indicated with different patterns of the bars. Each box in the box plots summarizes the estimated volumes with different CR and separates Trial 1 and 2. Note that the vertical axis does not start at 0.

4.2.2.2 Phantom Model B

The window settings used by the medical physicists (MP) when drawing the ROI on the PS images of phantom B is seen in Table 4.5. MP 1 and MP 2 drew twice, which is indicated by Trial 1 and Trial 2, whereas MP 3 only drew once. It can be observed that MP 1 and MP 3 adjusted the lower limit in the same way as when drawing the ROIs for phantom A, whereas MP 2 adjusted for the upper limit for all cases but also adjusted the lower limit in two of the cases. MP 3 used a higher lower limit than MP 1, for all cases.

Table 4.5: The window settings used by the MPs when drawing on PS scans of phantom B. The CR is shown for every measurement, indicated with different patterns on the bars. The upper and lower level show in percentage the limit chosen by the MPs, in relation to the maximum pixel value in each image. The MPs did draw twice (except MP 3), and this is shown as Trial 1 and Trial 2.

	Trial		**B**			
		Contrast	**11.9**	**7.2**	**6.6**	**5.0**
MP 1	**1**	**Upper**	100	100	100	100
		Lower	2	5	3	6
	2	**Upper**	100	100	100	100
		Lower	2	4	4	5
MP 2	**1**	**Upper**	87	94	97	93
		Lower	0	0	4	3
	2	**Upper**	93	92	91	98
		Lower	0	0	0	0
MP 3	**1**	**Upper**	100	100	100	100
		Lower	8	9	7	10
	2	**Upper**	-	-	-	-
		Lower	-	-	-	-

The volumes estimated, based on the drawn ROIs by the MPs on the PS images of phantom B are seen in Figure 4.5. The image with CR 7.2 (second bar) deviated the most for every MP. This was because of a suspected measurement error due to a larger detector-to-source distance, compared to the other measurements, resulting in a lower resolution. See the PS images in Appendix C for comparison. The volumes estimated from images with CR 7.2 were thus not included in the box plot. Without this measurement in consideration, the estimated phantom volume was smaller than the true phantom volume in all measurements, where MP 1 and 2 drew slightly the same and MP 3 drew smaller. For MP 1, the estimated volume from Trial 2 was smaller compared to the results from Trial 1. A reverse trend could be observed for MP 2. The deviation from the true volume presented in percentage is shown in Section 4.2.5 for all data.

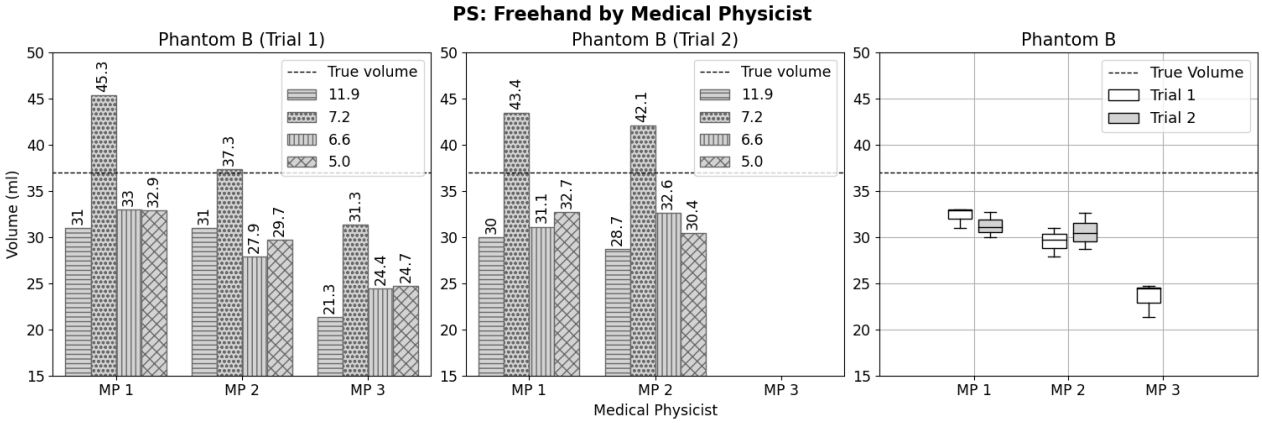

Figure 4.5: Phantom volumes estimated from ROIs drawn by freehand on PS images, by three medical physicists (MP 1 - 3). The true phantom volume is indicated by the dashed line. The CR for each image is indicated with different patterns of the bars. Each box in the box plots summarizes the estimated volumes with different CR and separates Trial 1 and 2. Note that the vertical axis does not start at 0, and that the CR 7.2 measurements are not included in the box plot.

4.2.3 Estimated Thyroid Phantom Volumes from Automatically Segmented PS Images

4.2.3.1 Phantom Models A

The volumes estimated from automatically segmented PS images of phantom models A are seen in Figure 4.6. There were fluctuations within each bar group (same phantom and threshold value, but different CR). For the smallest phantom (A2), the difference in CR was not as large as for the largest phantom (A4). Also, the estimated volume increased with decreasing CR. The spread of the estimated volumes (seen in the box plots) was smallest for phantom model A2, and the largest for phantom model A4. Overall, the different threshold values worked similar for all thyroid phantom sizes, where 25% worked best for A3 and A4. Note that the threshold values presented were simply chosen based on when the segmented volume best matched the true volume. This was performed with the purpose to find what threshold values implied in great estimated volumes. The deviation from the true volume presented in percentage is shown in Section 4.2.5 for all data.

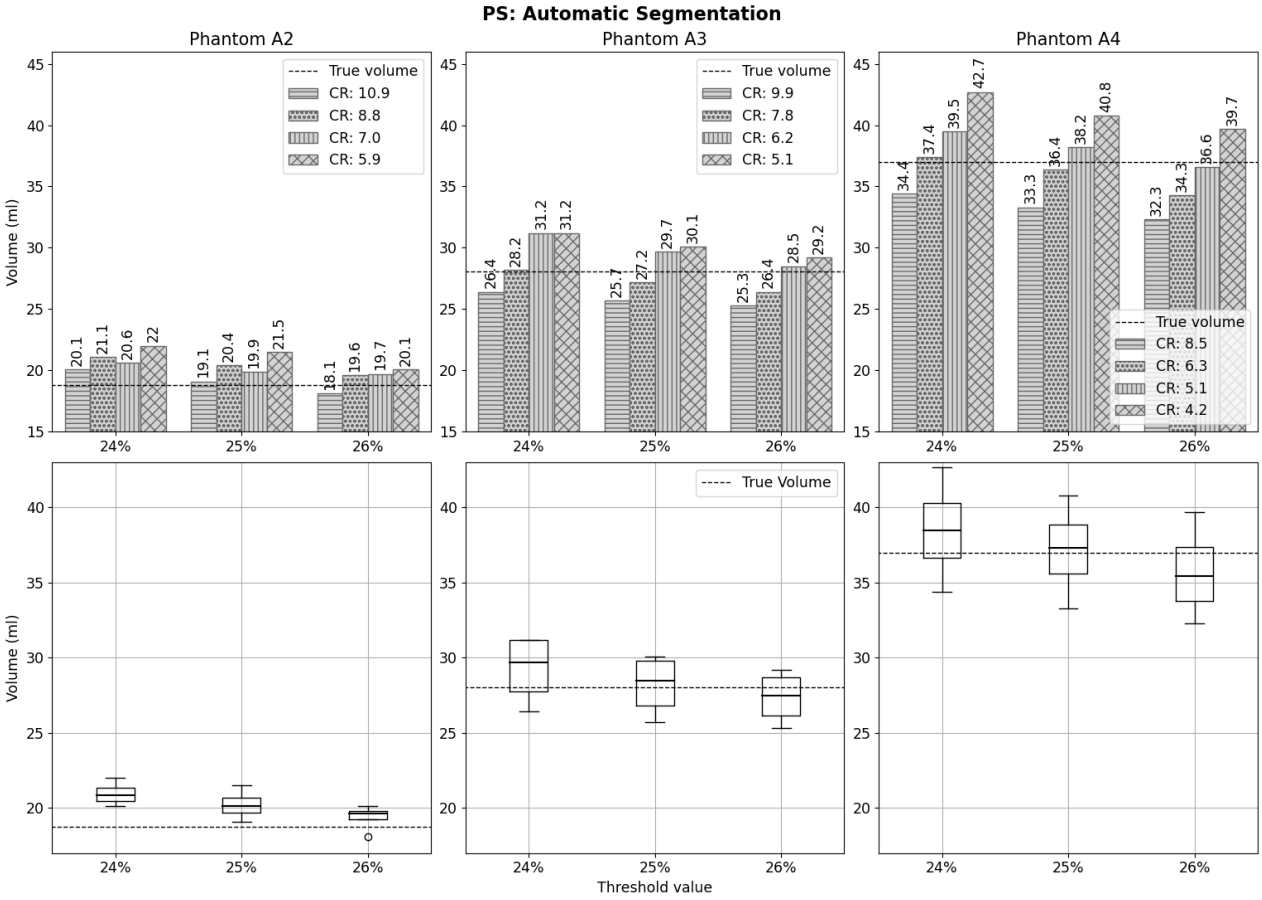

Figure 4.6: Phantom volumes estimated from automatically segmented PS images, with three different threshold levels. The true volume for each phantom is indicated by the dashed line. The CR for each image is indicated with different patterns of the bars. Each box in the box plots summarizes the estimated volumes with different CR. Note that the vertical axis does not start at 0.

4.2.3.2 Phantom Model B

The volumes estimated from automatically segmented PS images of phantom B are seen in Figure 4.7. The phantom volume estimated from the image with CR 7.2 (second bar) deviated much more from the true volume than for the other images, because of a suspected measurement error due to a misplaced detector. The volumes estimated from images with CR 7.2 were thus not included in the box plot. Excluding the CR 7.2 measurement indicated a trend towards larger estimated volumes for decreasing CR values. Estimated volumes also seemed to decrease with increasing threshold levels. Note that the threshold values presented were simply chosen based on when the segmented volume best matched the true volume. This was performed with the purpose to find what threshold values implied in great estimated volumes. The deviation from the true volume presented in percentage is shown in Section 4.2.5 for all data.

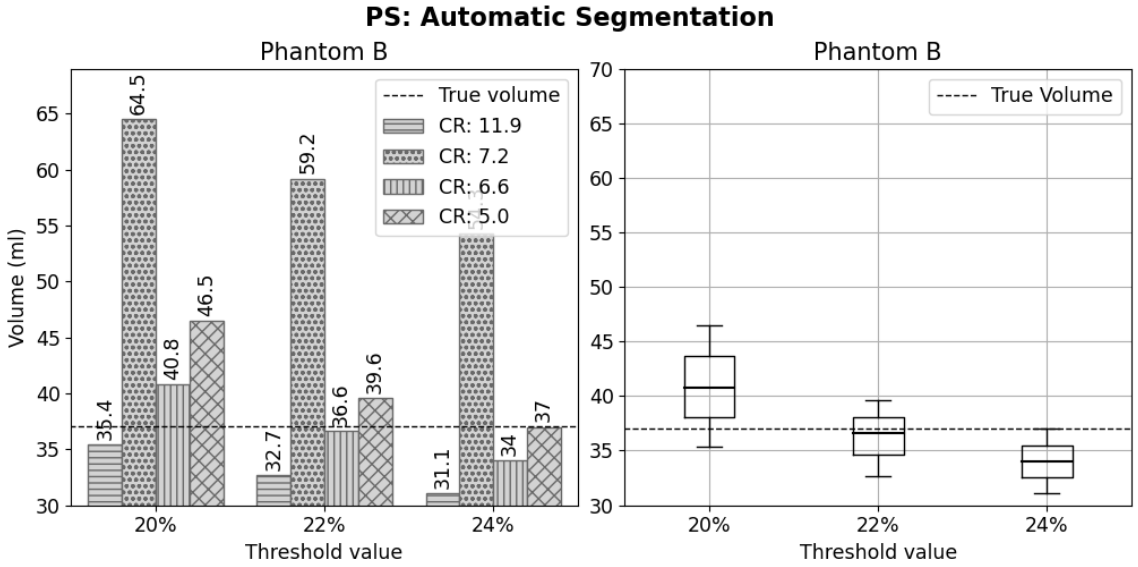

Figure 4.7: Phantom volumes estimated from automatically segmented PS images, with three different threshold levels. The true phantom volume is indicated by the dashed line. The CR for each image is indicated with different patterns of the bars. Each box in the box plots summarizes the estimated volumes with different CR. Note that the vertical axis does not start at 0, and that the CR 7.2 measurements are not included in the box plot.

4.2.4 Estimated Thyroid Phantom Volumes from Automatically Segmented SPECT Images

4.2.4.1 Phantom Models A

The volumes estimated from automatically segmented SPECT images of phantom models A are seen in Figure 4.8. There was not an as clear relationship between CR and estimated volume as it were for PS images (see Figure 4.6). Instead, the estimated volume decreased more with increasing threshold value. This pattern was more evident for the SPECT images compared to the PS images. Note that the difference in threshold value was 1% for the PS images and 4% for the SPECT images.

It was also observed that a higher threshold value (46%) seemed to fit better for a smaller phantom (A2) compared to a large phantom (A3 and A4). The opposite was that, a lower threshold value (38%) did fit better for larger phantoms (A3 and A4). Note that the threshold values presented were simply chosen based on when the segmented volume best matched the true volume. This was performed with the purpose to find what threshold values implied in great estimated volumes. The deviation from the true volume presented in percentage is shown in Section 4.2.5 for all data.

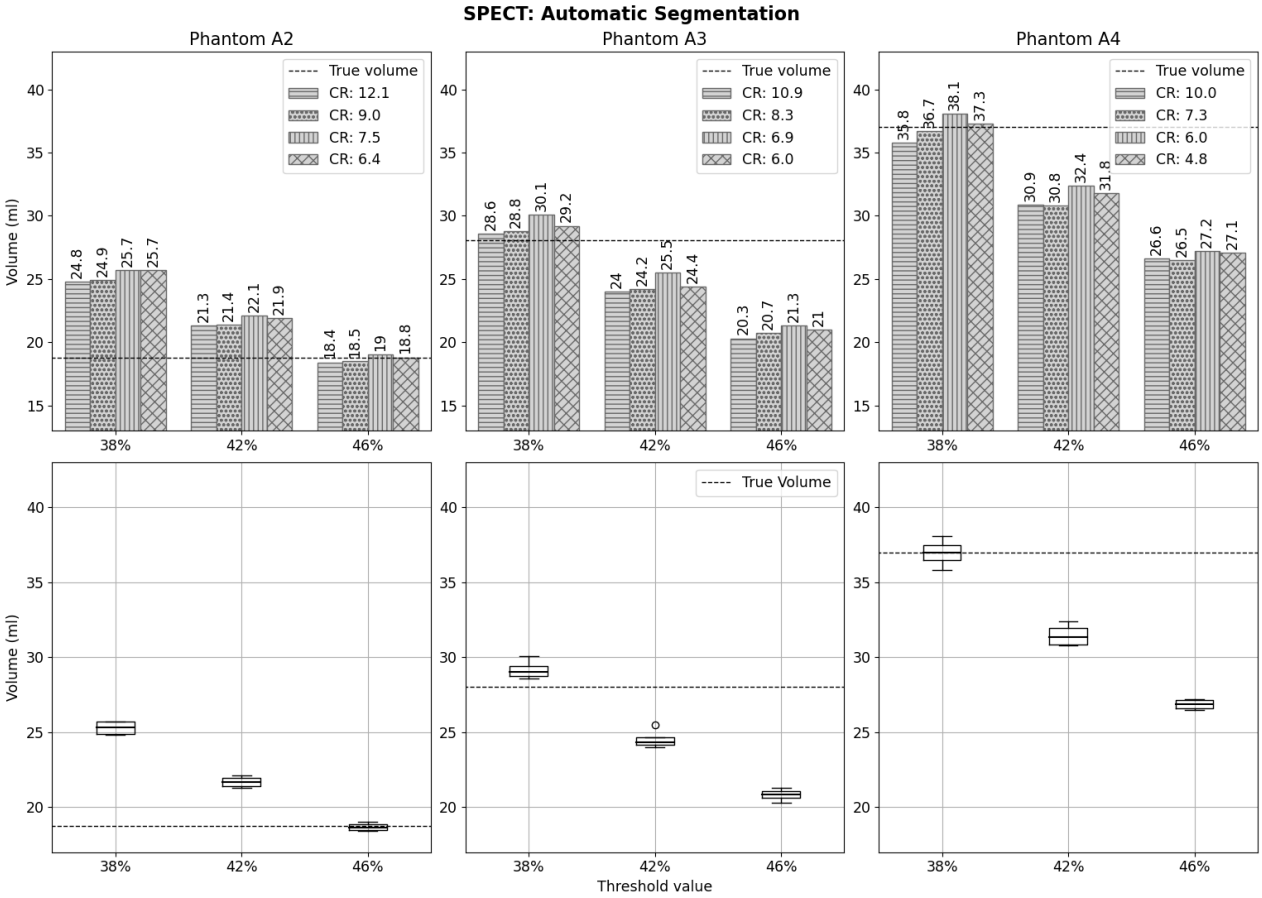

Figure 4.8: Phantom volumes estimated from automatically segmented SPECT images, with three different threshold values. The true volume for each phantom is indicated by the dashed line. The CR for each image is indicated with different patterns of the bars. Each box in the box plots summarizes the estimated volumes with different CR. Note that the vertical axis does not start at 0.

4.2.4.2 Phantom Model B

The volumes estimated from automatically segmented SPECT images of phantom B are seen in Figure 4.7. The estimated phantom volume seemed to be almost independent of the CR value.

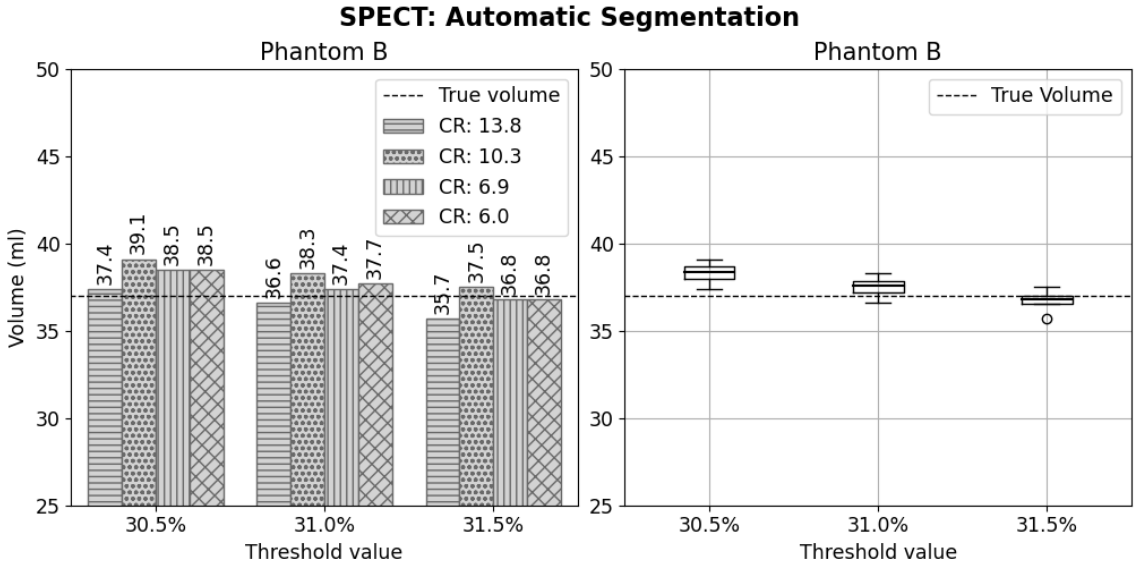

Figure 4.9: Phantom volumes estimated from automatically segmented SPECT images, with three different threshold values. The true phantom volume is indicated by the dashed line. The CR for each image is indicated with different patterns of the bars. Each box in the box plots summarizes the estimated volumes with different CR. Note that the vertical axis does not start at 0.

4.2.5 Summary of Estimated Phantom Volumes

The deviation between the median of the estimated phantom volume, by freehand, and the true phantom volume is seen in Table 4.6. Note that the median is for the grouped bars with the same phantom model and MP, but with different CR (as presented in the box plots). The deviation ranged from -35% to $+16\%$ with an overall negative deviation. This implied, according to Equation 2.6, that in the end, the administered activity to the patient may be up to 35% smaller or 16% larger than intended. Furthermore, the target dose is linear to the administrated activity, implying a target dose 35% less than expected. For example, an administrated activity of 600 MBq should result in an absorbed dose of 348 Gy to the thyroid gland, but if the volume is estimated with -35% deviation, the thyroid gland would receive an absorbed dose of only 226 Gy [24].

Table 4.6: Deviation (%) between the median of the estimated phantom volumes, from ROIs drawn by freehand by MPs on PS images, and the true phantom volume, for each phantom model A2, A3, A4 and B. The median is for the grouped bars (same phantom and MP, but different CR) for each phantom model .

	A2			**A3**			**A4**			**B**		
True volume (ml)	**18.8**			**28.1**			**37.0**			**37.0**		
MP	**1**	**2**	**3**	**1**	**2**	**3**	**1**	**2**	**3**	**1**	**2**	**3**
Trial 1: Median (ml)	16.7	21.9	17.0	22.4	29.2	22.7	26.5	35.4	27.1	32.9	29.7	24.2
Deviation (%)	−11	+16	−10	−20	+4	−19	−28	−4	−27	−11	−20	−35
Trial 2: Median (ml)	19.0	19.8	-	25.9	28.1	-	32.3	33.4	-	31.1	30.4	-
Deviation (%)	+1	+5	-	−8	0	-	−13	−10	-	−16	−18	-

The deviation between the median estimated phantom volume, from automatically segmented PS images, and the true phantom volume is seen in Table 4.7. Note that the median is for the grouped date with the same phantom model and threshold value, but with different CR (as presented in the box plots).

Table 4.7: Deviation (%) between the median of the estimated phantom volumes from automatic segmented PS images and the true phantom volume, for each phantom model A2, A3, A4 and B. The median is for the grouped bars (same phantom and threshold value, but different CR) for each phantom model .

	A2			**A3**			**A4**			**B**		
True volume (ml)	**18.8**			**28.1**			**37.0**			**37.0**		
Threshold (%)	**24**	**25**	**26**	**24**	**25**	**26**	**24**	**25**	**26**	**20**	**22**	**24**
Median (ml)	20.9	20.2	19.6	29.7	28.5	27.4	38.4	37.3	35.5	40.8	36.6	34.0
Deviation (%)	+11	+7	+4	+6	+1	−2	+4	+1	−4	+10	−1	−8

The deviation between the median estimated phantom volume, from automatically segmented SPECT images, and the true phantom volume is seen in Table 4.7. Note that the median is for the grouped date with the same phantom model and threshold value, but with different CR (as presented in the box plots).

Table 4.8: Deviation (%) between the median of the estimated phantom volumes from automatic segmented SPECT images and the true phantom volume, for each phantom model A2, A3, A4 and B. The median is for the grouped bars (same phantom and threshold value, but different CR) for each phantom model .

	A2			**A3**			**A4**			**B**		
True volume (ml)	**18.8**			**28.1**			**37.0**			**37.0**		
Threshold (%)	**38**	**42**	**46**	**38**	**42**	**46**	**38**	**42**	**46**	**30.5**	**31.0**	**31.5**
Median (ml)	25.3	21.7	18.7	29.0	24.3	20.9	37.0	31.4	26.9	38.4	37.6	36.8
Deviation (%)	+35	+15	−1	+3	−14	−26	0	−15	−27	+4	+2	−1

5 Discussion

5.1 Uptake Measurements

5.1.1 Source Position Dependence

The sensitivity curve for the detector was, to some extent, similar regardless of the type of source (Figure 4.1). As expected, there was a small difference between the sources of different sizes, but this occurred further away from the center of the detector and had therefore less effect on the RAIU value. However, from this data it could be concluded how well the detector needs to be centered over the thyroid to ensure that no volume of the thyroid is excluded from the measurement: if the center of the detector is misplaced relative to the center of the thyroid, by 5 cm, the RAIU value would still be above 90% compared with a perfect centered placement.

How well the detector is centered depends on the operator's experience and knowledge of the position of the thyroid gland in the neck. It is unlikely with a 5 cm shift of the detector position, therefore, it was assumed that a misalignment may result in an RAIU value less than 10% too low (taking only the position factor into account). However, operator-dependent detector placement was not investigated in this project. An endocrinologist would have had to be consulted for this.

Finally, the RAIU value cannot be overestimated if this factor alone is taken into account. An RAIU value with an deviation of -10% does imply a need to increase the administered activity with 11% (according to Equation 2.6) with a subsequent 11% raise in target dose.

5.1.2 Source Depth Dependence

As expected, the reduction in CPS increased with increasing source depth, i.e. with the thickness of the plexiglass above the source (Figure 4.2). However, the variations between thicknesses and between sources were not expected. This could be explained by the different types of plexiglass used for the measurements. With this explanation, this variation was not taken into account for final conclusions. Instead, the agreement between the experimental and theoretical trends was large, and there was no reason to believe that the experimental setup significant deviated from theory on this point.

If the main activity is 30 mm deep in the neck, this activity still contributes with up to 65% of its activity to the RAIU value. Without any specialist knowledge of thyroid anatomy, it is assumed that not all activity is this deep, but have a distribution in the entire gland. The RAIU value may deviate by up to -35% resulting in an administered activity and target dose that is 54% higher than expected.

5.1.3 Detector Angle Dependence

The detector angle had almost no influence on the sensitivity at the RAIU measurement (Figure 4.3). There were small variations observed for different angels, however, they may be explained by the handling of the detector between setups. The detector was moved when a new angle of the detector was set and this could have slightly affected the position of the detector. As mentioned above, the deviation of the detector sensitivity by different angles was less than 4%, and was thus

assumed to have a marginal affect on the RAIU value.

A redesigned experiment could have been performed in which the position-dependent sensitivity would have been investigated with different detector angles to obtain results as in Figure 4.1. As a result, the misplacement requirements (as stated in Section 5.1.1) could be different depending on the detector angle.

5.1.4 Air Gap Dependence

The detector-to-source distance was not the same without air gap as with an air gap, but the experimental measurements showed that this could be largely corrected for using the inverse square law. The air gap in the neck phantom seemed to have a major influence on the RAIU value, which was up to 27% higher without an air gap than with, if not distance corrected (Table 4.1). With distance correction, the deviation was 6%. However, the uptake measurement system does not correct for this air gap and in a clinical case, with an air gap, the RAIU value may be too low. Therefore, this is an important factor to consider when estimating the RAIU value in the clinic and how to reduce this deviation needs to be addressed. For example, the reference measurement should not be performed on a point source but rather on a source that better reflects the finite volume of a thyroid gland in a patient. In contrast to the other experimental uptake parameters studied (Sections 5.1.1-5.1.3), this factor results in a too low activity being administered to the patient, due to a higher RAIU value (according to Equation 2.1). An RAIU value deviation of 27% results in an administered activity and delivered target dose that are 21% lower of what is required to achieve the prescribed target dose.

5.2 Volume Estimation

5.2.1 CR Values

The extracted CR values from clinical cases (Table 4.2) had a larger range than the extracted CR values from phantom measurements (Table 4.3). The experimental CR values were within the range of the clinical CR values. Note that, in this project, the more prominent cases of GD and TA (CR values above 18) and the diffuse cases of TMNG (CR values below 5.0) were not investigated. However, visual assessment showed that the visual presentation of the image does not change with increasing CR value when the CR value is already high. Therefore, the ROIs drawn by freehand by the MPs should not be affected by very large CR values and the project was focused on lower CR values. On the other hand, the automatically segmented images were dependent by absolute values (threshold value) rather than visual representation of the thyroid appearance. The range of CR values in the experimental cases seemed to reflect the clinical cases, corresponding to the freehand drawn ROIs.

5.2.2 Window Settings

It was discovered that MP 2 did not follow the method description for adjusting the window settings (Table 4.4 and 4.5). For MP 2, the upper limit value was adjusted instead of the lower limit value. If the upper limit is lowered, the thyroid gland appears to be larger. If the lower limit is increased, as described in the method description, the thyroid gland appears smaller. MP 2 has therefore drawn larger ROIs compared to MP 1 and MP 3.

The window settings, used by the MPs when drawing on the PS images, appeared to correlate with the CR value. MP 1 and MP 3 used a higher lower limit for lower CR values. This is to be expected based on the method description, which emphasizes that the MP should adjust the lower limit until the background disappears. At a lower CR value, the background is more pronounced and the lower level needs to be raised more to make the background disappear, compared to with a higher CR value.

Furthermore, it appears that MP 1 did not adjust the lower limit in Trial 2 as much as in Trial 1. Similarly, MP 2 did not lower the upper limit in Trial 2 as much as in Trial 1. This may be due to an introduced bias between Trial 1 and Trial 2, since the MPs were allowed to observe and discuss the results of Trials 1 before performing Trial 2.

5.2.3 Estimated Volumes from Freehand Drawn ROIs

A clear bias could be observed between Trial 1 and Trial 2, for phantom models A (Figure 4.4). In Trial 1, MP 1 drew too small ROIs and thus too small volumes. However, after the presentation and discussion of the results, MP 1 drew larger ROIs in Trial 2. This pattern could be observed for each of the phantoms A2, A3 and A4, but most strongly for phantom A4. The opposite could be observed for MP 2, which drew smaller ROIs in Trial 2. In addition, MP 2 drew a smaller ROI for A4 in Trial 2, even though the estimated volume in Trial 1 was smaller than the true phantom volume. MPs were instructed to draw in Trial 2 with the same intention as in Trial 1 and as in clinical cases, despite the known results. However, they were unconsciously biased. Note that there was no bias for phantom B between Trials 1 and 2. However, the MPs drew all B images after they had been biased by Trial 1 of phantom models A.

Despite the bias between Trials 1 and 2, MP 1 and 3 appeared to have a relatively high precision. This also applied to the phantom model B (Figure 4.5). This was not as clear for MP 2, as the scatter of the estimated volume was larger with increasing phantom volume (for phantom models A).

There appeared to be no clear correlation between the CR value and the estimated volume. For example, MP 2 drew phantom A2 with CR=10.9 as the largest volume (22.9 ml) in Trial 1, but this was the smallest estimated volume in Trial 2 (19.1). This pattern could be observed in other images and for all MPs, particularly for phantom A4. This was also consistent with the previously mentioned non-correlation between CR value and window setting.

Unfortunately, there were no more phantom sizes available for comparison for model B, which reflect TA and TMNG. However, based on the results of phantom models A, it was to be expected that the estimated volumes should deviate more strongly with increasing phantom volume. Phantom model B also showed more intense hotspots compared to phantom models A (see Appendix C for comparison), which was to be expected. Note that phantom model A4 and B were identical except for the additional inner volumes in phantom B. However, the hotspots in phantom B implied a different intensity gradient compared to phantom models A. Therefore, the pixel value level the MPs followed, for the ROI drawing, was also affected and thus the estimated volume.

In the case of TA and TMNG, where the entire thyroid gland is not overactive but nodules are, the question also arises as to how much of the area should be taken into account when estimating the thyroid volume. It was clear from this project that the high intensity patches affect the appearance of the thyroid gland and therefore the estimated volume. If some parts of the thyroid gland are not included in the drawing, this does not mean that this volume will not receive an absorbed dose.

The estimated volumes depended on the drawn ROIs. While the drawing process can be investigated and improved, the precision and accuracy of the estimated volumes will only be improved if the transformation from ROI area to thyroid volume is accurate. That is, a ROI may be perfectly drawn in terms of correctly identifying the thyroid margin in the image, but if the relation between ROI area and thyroid volume is not well known, instead the ROI may be assumed to be incorrectly drawn.

Finally, as explained in section 4.2.5, the relationship between estimated volume and administered activity is linear, as is the relationship between administered activity and target dose. The data obtained in this project therefore showed that a patient at HSH may receive up to 35% less target dose than expected, with the assumption of a correct estimated RAIU value. On the other hand, a patient may also receive an excessive target dose of 16%. However, these are the maximum deviation values evaluated in this project and should not be considered as typical values. In addition, the number of phantom models (to size and design), CR values and repeated trials could have been increased in order to draw more significant conclusions. In particular, the clinical variation in the appearance of TMNG is large, and phantom model B was just one example. However, investigating a wider variation of designs could further improve the volume estimation procedure at HSH.

5.2.4 Estimated Volumes from Automatic Segmentation

The estimated volumes from automatically segmented PS and SPECT images were performed to get an idea of how these estimated volumes differ from those based on freehand drawn ROIs, as well as the main differences between estimated volumes from automatically segmented PS and SPECT images. As these methods are not used in the clinic, no parallels are drawn between the method and the target dose delivered to the thyroid gland. Furthermore, no optimization of the scanning protocols was performed as it was of interest to investigate the estimated volumes based on the current protocols and to compare PS and SPECT.

The main difference between the estimated volumes, based on PS and SPECT images, was that there was almost no dependence on the CR value in the segmented SPECT images, while CR had a large influence in the segmented PS images. This could be due to the fact that a pixel and its pixel value in a PS image represents the number of pulses in the entire thickness. Thus, pulses from the background are added to the thyroid region. Also, the maximum pixel value is included with pulses from the background, and a change in background activity changes the CR value as well as the maximum pixel value. In the reconstructed and sliced SPECT image, a pixel and its pixel value represent only this one position without pulses from the background (ideally). Therefore, the automatic segmentation of SPECT images was not as sensitive to fluctuations in background activity.

The second main difference between the estimated volumes based on PS and SPECT images was

that PS segmentation was less sensitive to changes in threshold value than SPECT segmentation, which varied greatly depending on the threshold value. This is because the profile of a PS image has as a rounded shape, whereas the SPECT image is reconstructed and sliced, producing a rectangular profile with a sharp edge. A small change in the threshold value does not change the line of segmentation as much on a rounded edge as on a sharp edge.

6 Conclusions

6.1 RAIU Value

The deviation of the RAIU value may be 10% lower if the detector is misplaced up to 5 cm from the center of the thyroid gland. This would result in an 11% higher target dose to the patient. Moreover, with a deep lying thyroid gland, the RAIU value may become 35% too small, resulting in a 54% higher target dose. The RAIU value may also deviate by up to 27% due to the presence of an air gap at the reference measurement, resulting in a 21% lower target dose. This can be avoided by adjusting the setup. The angle of the detector had less influence on the RAIU value provided that the detector FOV was centered over the thyroid gland.

6.2 Estimated Phantom Volumes

The estimated phantom volumes differed between the medical physicists at HSH, with two of them drawing significantly smaller volumes than the actual volume and the third drawing larger volumes. The window settings used when drawing the ROIs had a large influence on the final estimated volumes, while the count ratio between the thyroid phantom and the background appeared to have no correlation with the estimated phantom volume. The maximum recorded deviation of the estimated volume was 35% less than the actual volume, but smaller deviations were more frequent, resulting in a maximum target dose deviation of 35%. Overall, the precision was higher than the accuracy.

The main differences between automatically segmented planar scintigraphic and SPECT images were how the methods were affected by the segmentation threshold and CR. Planar segmentation of scintigraphic images was found to be more sensitive to different CR, while SPECT images were more sensitive to different thresholds.

7 Future Work

It could be investigated how operator-dependent and the radioiodine uptake measurement is by investigating how well the detector FOV is centered over the thyroid gland. In addition, the setup dependence could be further investigated. The method for estimating thyroid volume may presumably be improved at HSH to ensure more accurate target doses to the patient. The phantoms used in this project were few and the combinations of background and phantom radioiodine concentrations need to be extended. It can also be further investigated whether the operator-dependent factor in drawing freehand ROIs is too large or whether an automatic segmentation method should replace the freehand drawing method. If so, it needs to be evaluated which type of image acquisition method (planar scintigraphy or SPECT) should be used as a basis, which threshold value and if there has to be different methods depending on diagnosis. Overall, there are more factors influencing the uncertainty of the final delivered target dose that could be further investigated.

References

[1] Sköldkörtelförbundet. Hypertyreos – överfunktion i sköldkörteln [Internet]. Stockholm: Sköldkörtelförbundet; [date unkown][cited 2024 January 29]. Available from: https://skoldkortelforbundet.se/om-skoldkortelsjukdom/hypertyreos/.

[2] Filipsson Nyström H. Nationellt vårdprogram för hypertyreos. Stockholm: Den nationella arbetsgruppen; 2022.

[3] De Leo S, Lee SY, Braverman LE. Hyperthyroidism. Lancet. 2016 Aug 27;388(10047):906-918. doi: 10.1016/S0140-6736(16)00278-6. Epub 2016 Mar 30. PMID: 27038492; PMCID: PMC5014602.

[4] Campennì A, Avram AM, Verburg FA, Iakovou I, Hänscheid H, de Keizer B, Petranović Ovčariček P, Giovanella L. The EANM guideline on radioiodine therapy of benign thyroid disease. Eur J Nucl Med Mol Imaging. 2023 Sep;50(11):3324-3348. doi: 10.1007/s00259-023-06274-5. Epub 2023 Jul 3. PMID: 37395802; PMCID: PMC10542302.

[5] Eckerman K, Endo A. MIRD: Radionuclide Data and Decay Schemes. 2 ed. Baltimore: Alien Bindings; 2008.

[6] Mattsson S, Johansson L, Jönsson H, Nosslin B. Radioactive iodine in thyroid medicine–how it started in Sweden and some of today's challenges. Acta Oncol. 2006;45(8):1031-6. doi: 10.1080/02841860600635888. PMID: 17118834.

[7] Läkemedelsverket. Ultra-TechneKow FM 2,15-43 GBq radionuklidgenerator [Internet]. Stockholm: Läkemedelsverket; [date unkown][cited 2024 February 20]. Avaibable from: https://www.lakemedelsverket.se/sv/sok-lakemedelsfakta/lakemedel/19900302000020/ultra-technekow-fm-2-15-43-gbq-radionuklidgenerator.

[8] Cleveland Clinic. Graves' Disease [Internet]. Ohio: Cleveland Clinic; c2024 [cited 2024 March 7]. Available from: https://my.clevelandclinic.org/health/diseases/15244-graves-disease.

[9] Cleveland Clinic. Thyroid Nodules [Internet]. Ohio: Cleveland Clinic; c2024 [cited 2024 March 7]. Available from: https://my.clevelandclinic.org/health/diseases/13121-thyroid-nodule.

[10] Wikimedia Commons. Thyroid gland [illustration]. 2019 [cited 2024 April 2]. Available from: https://commons.wikimedia.org/wiki/File:Thyroid_gland_la.svg.

[11] Cleveland Clinic. Thyroid [Internet]. Ohio: Cleveland Clinic; c2024 [cited 2024 March 7]. Available from: https://my.clevelandclinic.org/health/body/23188-thyroid.

[12] ICRP. Publication 23, Report of the Task Group on Reference Man [Internet]. New York: ICRP; 1992. 74; 29476 [cited 2024 March 28]. Available from: https://journals.sagepub.com/pb-assets/cmscontent/ANI/P_023_1975_Report_on_the_Task_Group_on_Reference_Man_rev0.pdf.

[13] Cleveland Clinic. Thyroiditis [Internet]. Ohio: Cleveland Clinic; c2024 [cited 2024 April 27]. AVailable from: https://my.clevelandclinic.org/health/diseases/15455-thyroiditis.

[14] Giovanella L, Avram AM, Iakovou I, Kwak J, Lawson SA, Lulaj E, Luster M, Piccardo A, Schmidt M, Tulchinsky M, Verburg FA, Wolin E. EANM practice guideline/SNMMI procedure standard for RAIU and thyroid scintigraphy. Eur J Nucl Med Mol Imaging. 2019 Nov;46(12):2514-2525. doi: 10.1007/s00259-019-04472-8. Epub 2019 Aug 7. PMID: 31392371.

[15] Gammadata Instrument AB. Captus 4000 – Thyroidea Upptagssystem [Internet]. Uppsala: Gammadata Instrument AB [date unkown; cited 2024 May 9]. Available from: `https://gammadata.se/sv/produkt/radioaktivitetsmaetning/sjukhusfysik/upptagsmatning/captus-4000-thyroidea-upptagssystem/`.

[16] Capintec, Inc.. Captus 4000e Thyroid Uptake System, Owner's manual. No. 9250-0151. 2017 June 28.

[17] Huang JY, Lin KJ, Chen YS. Fully automated computer-aided volume estimation system for thyroid planar scintigraphy. Comput Biol Med. 2013 Oct;43(10):1341-52. doi: 10.1016/j.compbiomed.2013.07.006. Epub 2013 Jul 15. PMID: 24034725.

[18] Calandri E, Giraudo MT, Sirovich R, Ostan A, Pultrone M, Frantellizzi V, Conversano L, Bagnasacco P, Gallina S, Vincentis G. Usefulness of 99mTc-Pertechnetate SPECT-CT in Thyroid Tissue Volumetry: Phantom Studies and a Clinical Case Series. Curr Radiopharm. 2022;15(3):205-217. doi: 10.2174/1874471015666220111145550. PMID: 35021984.

[19] Petros Perros. Thyroid scintigraphy [illustration]. 2005 [cited 2024 April 2]. Available from: `https://commons.wikimedia.org/wiki/File:Thyroid_scintigraphy.jpg`.

[20] HIMANKA E, LARSSON LG. Estimation of thyroid volume; an anatomic study of the correlation between the frontal silhouette and the volume of the gland. Acta radiol. 1955 Feb;43(2):125-31. PMID: 14376125.

[21] Zaidi H. Comparative methods for quantifying thyroid volume using planar imaging and SPECT. J Nucl Med. 1996 Aug;37(8):1421-6. PMID: 8708788.

[22] Marinelli LD, Quimby EH, Hine GJ. Dosage determination with radioactive isotopes; practical considerations in therapy and protection. Am J Roentgenol Radium Ther. 1948 Feb;59(2):260-81. PMID: 18905884.

[23] Jönsson H, Mattsson S. Single uptake measurement for absorbed dose planning for radioiodine treatment of hyperthyroidism. Cancer Biother Radiopharm. 2003 Jun;18(3):473-9. doi: 10.1089/108497803322285233. PMID: 12954135.

[24] Strålsäkerhetsmyndigehten. Doskatalog [Internet]. Stockholm: Strålsäkerhetsmyndigheten; 2021 [updated 2021 February 12; cited 2024 May 9]. Available from: `https://www.stralsakerhetsmyndigheten.se/omraden/stralning-i-varden/doskatalog/`.

[25] Läkemedelsverket. Natriumjodid (I-131) GE Healthcare 333-3700 kBq kapsel, hård [Internet]. Stockholm: Läkemedelsverket; [date unknown][cited 2024 March 25]. Available from: `https://www.lakemedelsverket.se/sv/sok-lakemedelsfakta/lakemedel/19900621000190/natriumjodid-i-131-ge-healthcare-333-3700-kbq-kapsel-hard`.

[26] Liu B, Huang R, Kuang A, Zhao Z, Zeng Y, Wang J, Tian R. Iodine kinetics and dosimetry in the salivary glands during repeated courses of radioiodine therapy for thyroid cancer. Med Phys. 2011 Oct;38(10):5412-9. doi: 10.1118/1.3602459. PMID: 21992360.

[27] Taprogge J, Gape PMD, Carnegie-Peake L, Murray I, Gear JI, Leek F, Hyer SL, Flux GD. A Systematic Review and Meta-Analysis of the Relationship Between the Radiation Absorbed Dose to the Thyroid and Response in Patients Treated with Radioiodine for Graves' Disease. Thyroid. 2021 Dec;31(12):1829-1838. doi: 10.1089/thy.2021.0302. PMID: 34598656; PMCID: PMC8721505.

[28] Jessen L, Gustafsson J, Ljungberg M, Curkic-Kapidzic S, Imsirovic M, Sjögreen-Gleisner K. 3D printed non-uniform anthropomorphic phantoms for quantitative SPECT. EJNMMI Phys. 2024 Jan 22;11(1):8. doi: 10.1186/s40658-024-00613-7. PMID: 38252205; PMCID: PMC10803701.

[29] Segars WP, Sturgeon G, Mendonca S, Grimes J, Tsui BM. 4D XCAT phantom for multi-modality imaging research. Med Phys. 2010 Sep;37(9):4902-15. doi: 10.1118/1.3480985. PMID: 20964209; PMCID: PMC2941518.

Appendix A Gamma Camera Settings and Acquisitions Parameters

The gamma camera settings and acquisition parameters, used for thyroid scintigraphy at the Nuclear Medicine Clinic at HSH, can be seen in Table A.1. The same settings and parameters were used for the experimental scintigraphy, but with an halved acquisition time to save time (300 seconds insted of 600 seconds for PS and 15 seconds per projection insted of 30 seconds for SPECT). Because of this, the injected activity of technetium pertecnetate to the phantom was doubled in relation to what was expecting to be in the patients' thyroid gland.

Table A.1: The gamma camera settings and acquisition parameters used for planar scintigraphy and SPECT of the thyroid gland at the Nuclear Medicine Clinic at HSH. The same settings and parameters were used for the experimental scintigraphy scans, but with adjusted acquisition time (clinical / experimental).

PS	Camera setup	H-mode, 0°(static)
	Collimator	LEHR (low energy, high resolution)
	Active detecors	1 (0°)
	Stop at acquisition time	600 seconds / 300 seconds
	Stop at count	500 000 counts / -
	Matrix size	128x128
	Zoom	1.6
	Energy window	140.6 keV ± 10%
SPECT	Camera setup	H-mode
	Collimator	LEHR (low energy, high resolution)
	Active detecors	1
	Acquisition process	Step and shot
	Start angle	180°
	Scan arc	360°
	Angular step	6°
	Number of projections	60
	Acquisition time per projection	30 seconds / 15 seconds
	Matrix size	128x128
	Zoom	1.5
	Energy window	140.6 keV ± 10%
	Reconstruction method	OSEM
	Number of subsets	10
	Number of iterations	2
	Filter	Butterworth
	Critical frequency	0.48 $(\text{px}\cdot\text{mm})^{-1}$
	Power	10

Appendix B Matrix for Uptake Measurements

The matrix used for position guidance during the uptake measurements.

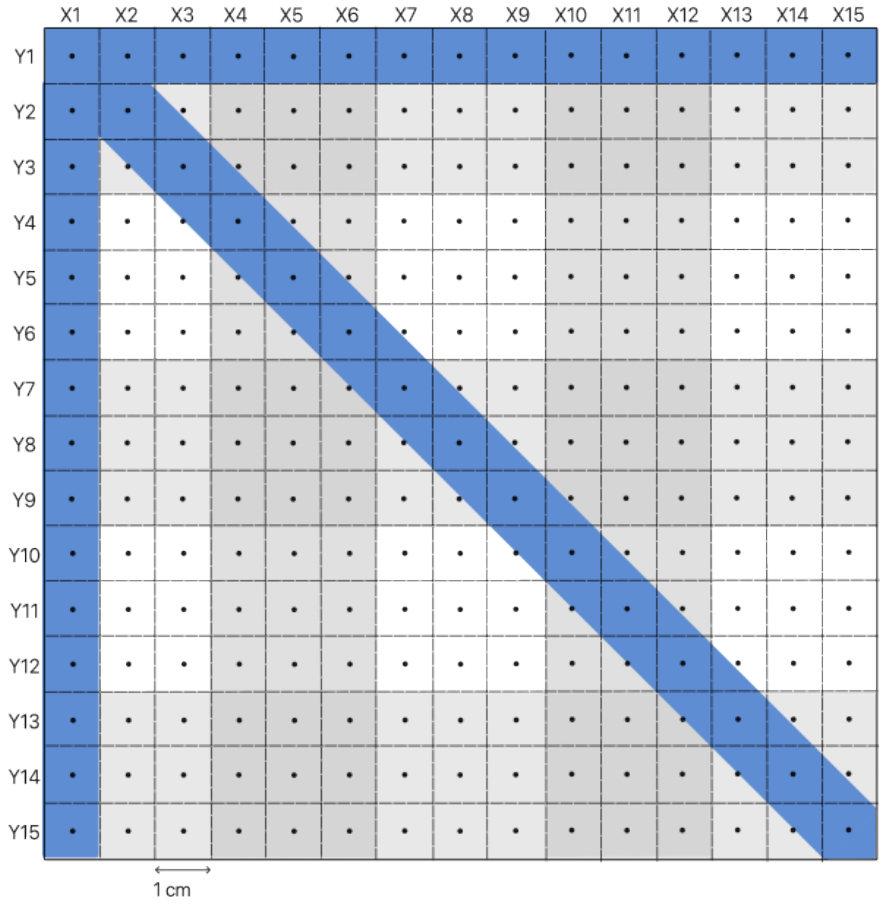

Figure B.1: The matrix used for guidance for the source position during the experimental uptake measurements. The detector was centered at position X1, Y1. The blue elements show the positions used for measurements. Each element is 1x1 cm^2.

Appendix C Planar Scintigraphic Images

The extracted planar scintigraphic images, used as material for the volume estimation with freehand drawn ROIs and with automatic segmenting method.

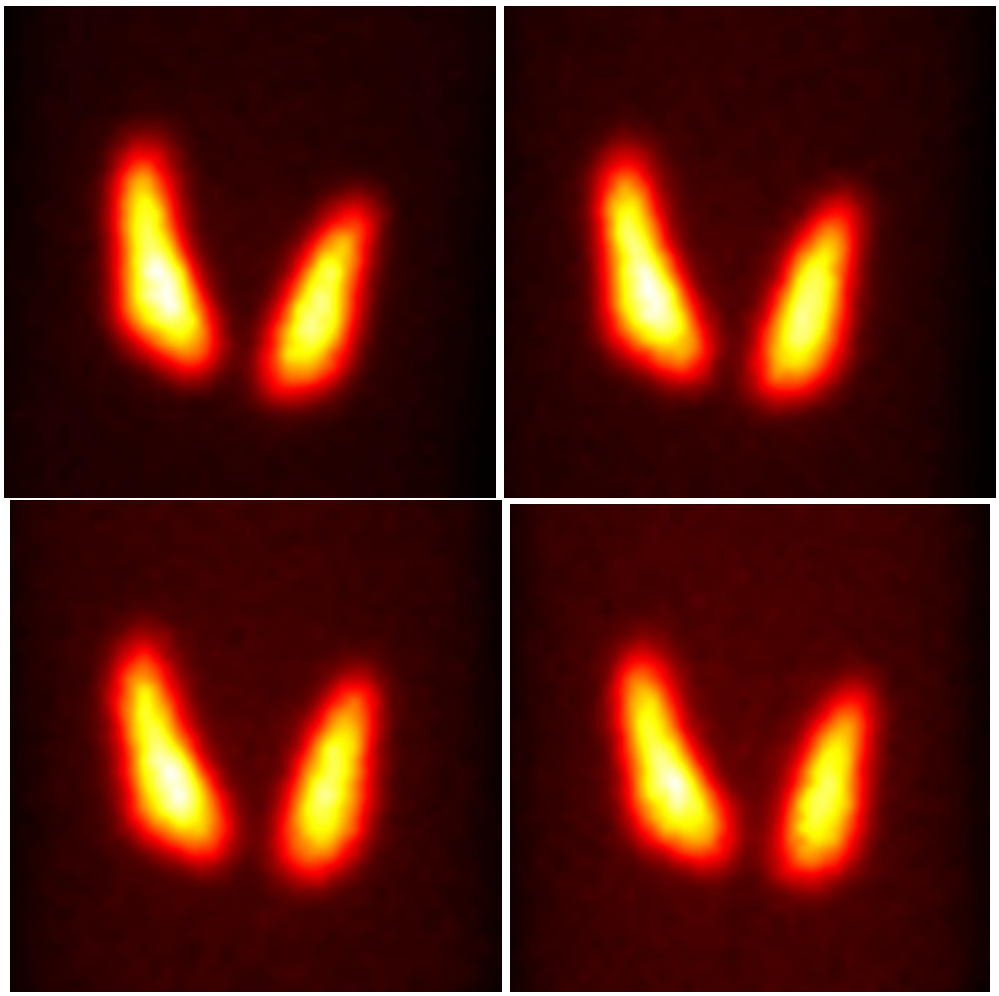

Figure C.1: PS images of phantom model A2, with CR values 10.9, 8.8, 7.0 and 5.9. Original window settings.

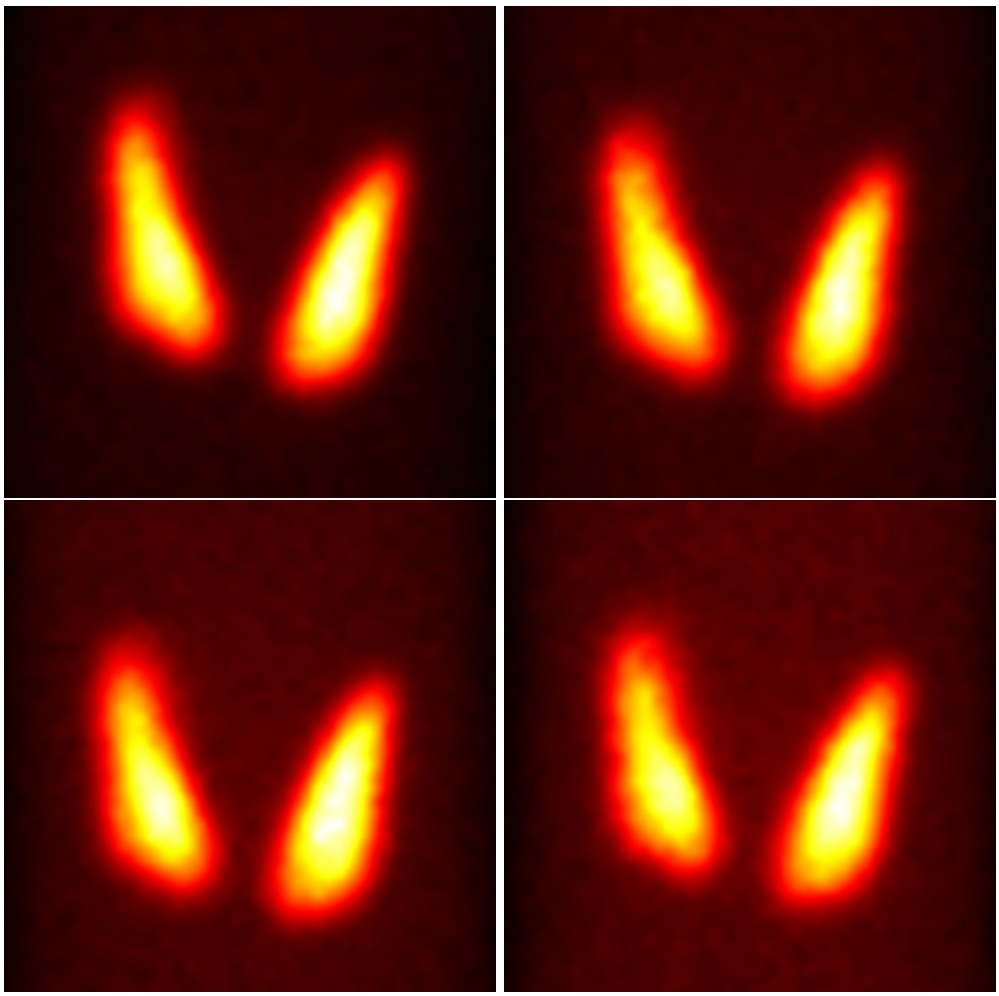

Figure C.2: PS images of phantom model A3, with CR values 9.9, 7.8, 6.2 and 5.1. Original window settings.

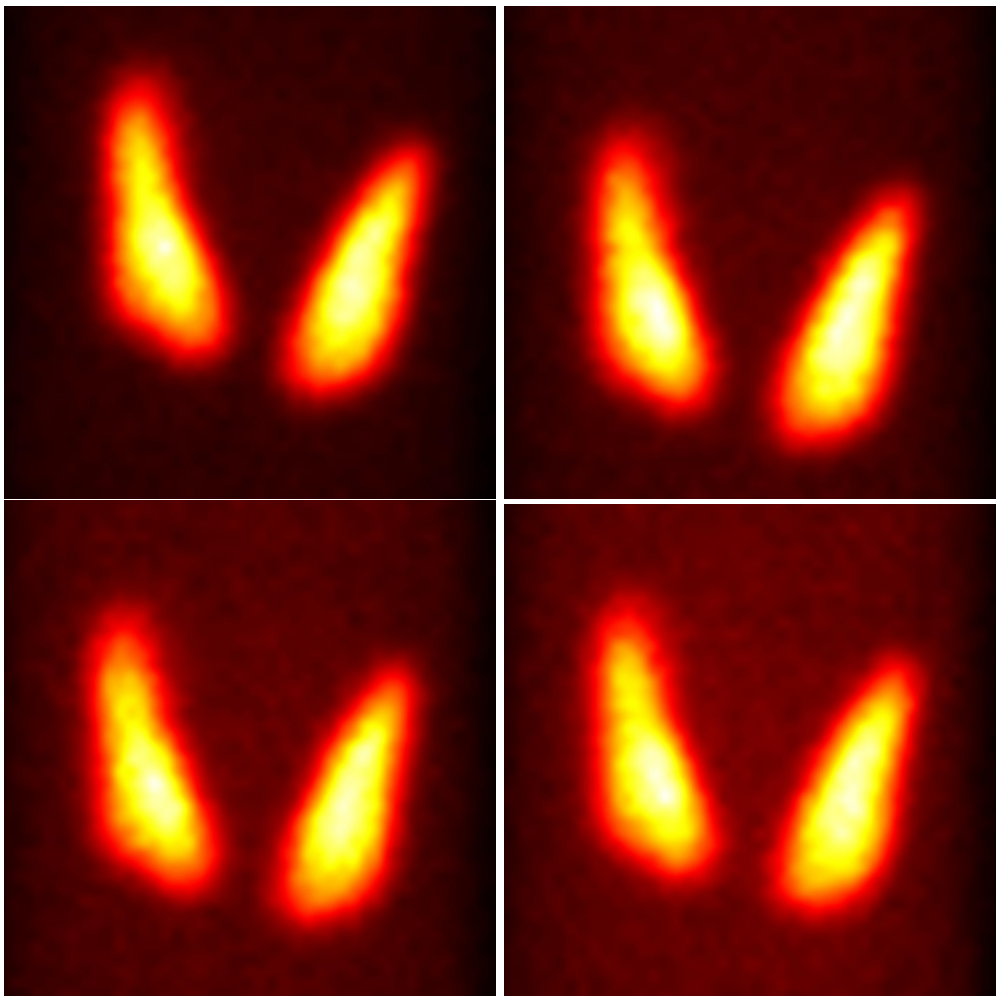

Figure C.3: PS images of phantom model A4, with CR values 8.5, 6.3, 5.1 and 4.2. Original window settings.

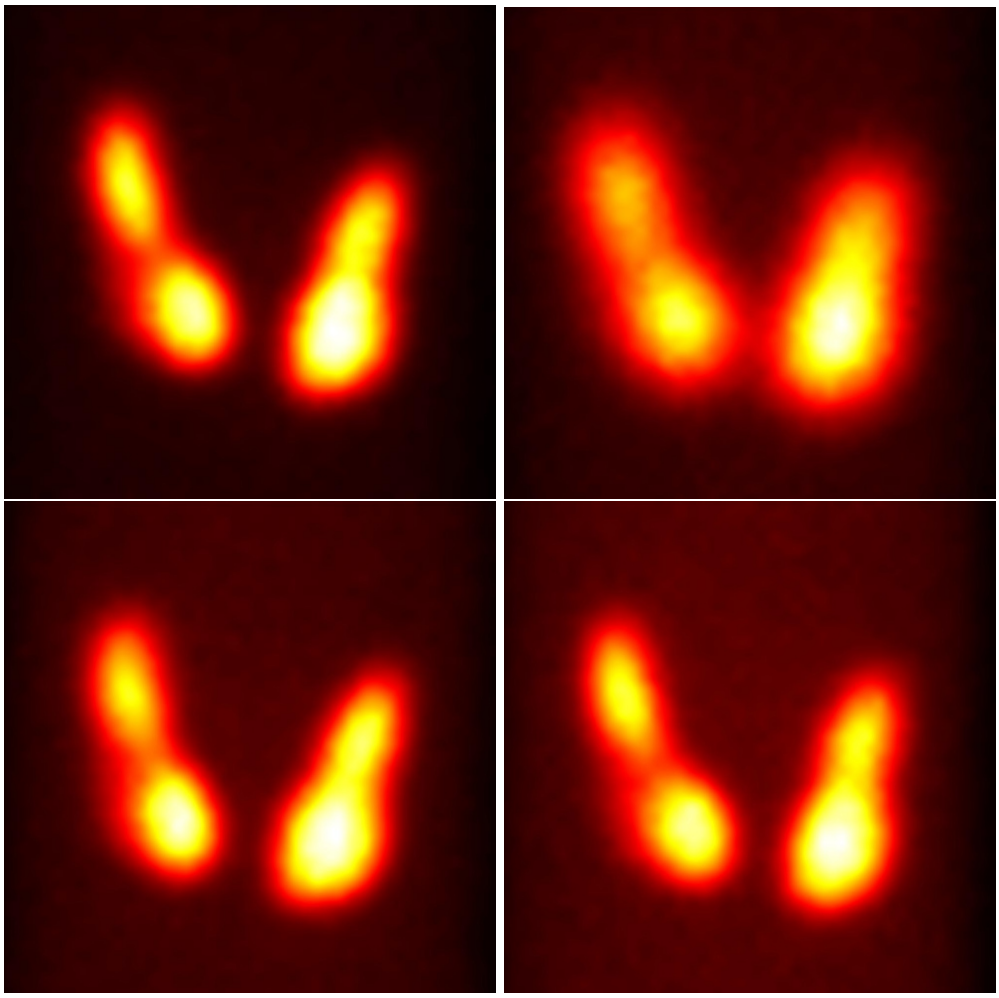

Figure C.4: PS images of phantom model B, with CR values 11.9, 7.2, 6.6 and 5.0. Original window settings.